Design of a high pulse energy coherent ultraviolet source – simulations and experimental design

Gunnar Rustad and Øystein Farsund

Norwegian Defence Research Establishment (FFI)

1 February 2013

FFI-rapport 2013/00372

117901

P: ISBN 978-82-464-2209-1
E: ISBN 978-82-464-2210-7

Keywords

Ikke-lineær optikk

Modellering og simulering

Lasere

Optiske materialer

Laserteknikk

Approved by

Knut Stenersen	Project Manager
Johnny Bardal	Director

English summary

The report discusses design considerations and numerical simulations of different system architectures for generation of several tens of mJ pulse energy in the ultraviolet range around 290-300 nm. The architectures considered are based on a pulsed 1 μm pump laser and nonlinear optical conversion to reach the ultraviolet. The simulations have been done using FFI's sophisticated simulation tool, SISYFOS, taking into account all relevant physical effects in the conversion processes. Two different pathways, which were identified as the most promising in a previous FFI-report [1], have been studied. Pathway 1 includes sum frequency generation (SFG) of 355 nm and 1650 nm, while pathway 2 utilizes SFG of 532 nm and 650 nm. The 1650 nm and 650 nm beams are generated through frequency down conversion of 1064 nm and 532 nm beams, respectively, in an optical parametric oscillator (OPO). Both pathways and the main nonlinear conversion stages of each of them have been studied in detail.

The dimensioning factor in the simulations has been the output from an available commercial pump laser. This is capable of delivering 600 mJ at 1064 nm or, with harmonic generation stages, 200 mJ at 532 nm or 170 mJ at 355 nm. It was found for both pathways that 120 mJ should be used to pump the OPO and the rest of the available energy to be used in the sum frequency stage. The design of an OPO with high conversion efficiency and high beam quality that is pumped with more than 100 mJ is challenging. A novel architecture that uses the far-field limiting properties of two different nonlinear crystals in the same OPO is described. OPOs based on this architecture are capable of giving sufficiently high beam quality for the high energy beams. For comparison, a considerably more complicated master-oscillator power-amplifier (MOPA) is also studied. Simulations show that this architecture can perform slightly better, but the far simpler experimental layout of the OPO makes this still the recommended choice for the down-conversion stage.

Simulations show that both pathways are capable of generating ~80 mJ at 290-300 nm starting from a single-frequency 600 mJ 1 μm pump source. The beam quality at the ultraviolet wavelength is expected to be M^2~2-4, where the beam quality from pathway 1 is slightly better than from pathway 2. It is further shown that the SFG-process is sensitive to the bandwidth of the pump laser, and that the expected output energy would decrease to 40-50 mJ when using a pump laser with 20 GHz bandwidth.

Sammendrag

Rapporten tar for seg design av to ulike systemarkitekturer som kan benyttes til generering av ultrafiolette laserpulser med flere titalls millijoule energi i bølgelengdeområdet 290-300 nm. Systemarkitekturene baserer seg på ikkelineær optisk konvertering av en pulset 1 µm laser og ble pekt ut som de mest lovende for dette formålet i en tidligere FFI-Rapport [1]. Arbeidet inkluderer omfattende numeriske simuleringer som har brukt FFIs avanserte egenutviklede simuleringsverktøy, SISYFOS. Dette simuleringverktøyet inkluderer alle relevante fysiske effekter i konverteringsprosessene.

Arkitektur 1 bruker sumfrekvenskonvertering (SFG) av 355 nm og 1650 nm, mens arkitektur 2 bruker SFG av 532 nm og 650 nm. Strålene med 650 nm og 1650 nm lys er generert ved frekvensnedkonvertering av hhv 532 nm og 1064 nm i en optisk parametrisk oscillator (OPO). Begge systemarkitekturer og de viktigste ikkelineære konverteringstrinnene er studert i detalj.

Som dimensjonerende faktor for simuleringene er det brukt energien fra en kommersielt tilgjengelig pumpelaser. Denne kan gi 600 mJ ved 1064 nm, eller 200 mJ ved 532 nm eller 170 mJ ved 355 nm hvis laserens utstyr for harmonisk generering benyttes. Det ble funnet for begge arkitekturer at 120 mJ av det tilgjengelige pumpelyset skulle brukes til å pumpe OPO-trinnet og at resten av pumpeenergien skulle brukes i SFG-trinnet. Design av en effektiv OPO med god strålekvalitet som er pumpet med mer enn 100 mJ er utfordrende. En nyutviklet og enkel metode som benytter de fjernfeltbegrensende egenskapene til to ulike ikkelineære krystaller i samme OPO er beskrevet. OPOer basert på denne arkitekturen er i stand til å gi tilstrekkelig høy strålekvalitet for 650 nm og 1650 nm strålene i dette arbeidet. For sammenligning er også master-oscillator – power amplifier (MOPA) arkitekturer for dette konverteringstrinnet studert. Disse er betydelig mer kompliserte å realisere eksperimentelt. Simuleringene viste at en MOPA ga en noe bedre ytelse enn en OPO, men OPOen ble fortsatt anbefalt for videre studier pga den betydelig enklere eksperimentelle utformingen.

Simuleringnen viste at begge arkitekturer har potensial for generering av ca 80 mJ ved 290-300 nm hvis man starter med 600 mJ fra en singel-frekvens laser. Forventet strålekvalitet er i området M^2 ~2-4, hvor strålekvaliteten fra arkitektur 1 er best. Det er videre vist at effektiviteten til det ikkelineære SFG-trinnet er følsomt for båndbredden til pumpelaseren og at forventet utenergi vil synke til 40-50 mJ ved 20 GHz pumpebåndbredde.

Contents

1 Introduction

One of the main objectives for Project 1179 is to develop an ultraviolet laser source with high pulse energy. In a previous report [1], different architectures for efficient conversion from 1064 nm to 290 nm were reviewed and the two most promising architectures were identified. These are shown in Figure 1.1.

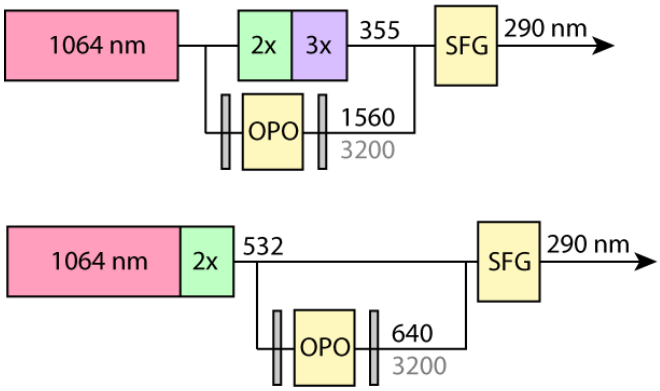

Figure 1.1 Sketch of the two architectures that are studied in this work. OPO – Optical parametric oscillator, SFG – Sum frequency generation, 2x – Second harmonic generation, 3x – Third harmonic generation. The numbers indicate wavelengths in nanometers

In this report, these architectures are studied in detail by advanced numerical simulations where pump beam size, crystal lengths, output coupling in addition to resonator design are varied to optimize the performance, i.e. the nonlinear conversion efficiency and the output beam quality. In addition, parameters such as crystal size and peak fluence must have feasible values.

It should be noted that compared to Figure 1.1, the wavelength of the output from the OPO stage (and input to the SFG stage) may need to be somewhat longer because of absorption properties in the 3 µm range of some of the nonlinear materials. The resulting ultraviolet wavelength will then be somewhat longer, for instance if the wavelength from the OPO in architecture 1 is 1700 nm (instead of 1560 nm), the resulting wavelength after SFG is 293.7 nm.

In Chapter 2, the simulation model is described, while the considerations to be made in the simulations are explained in Chapter 3. Simulations and optimization of the different OPOs and MOPAs are presented in Chapter 4, while the final SFG is presented in Chapter 5.

2 Description of simulation model

2.1 The SISYFOS simulation model

All the numerical simulations performed in this work use the SISYFOS simulation model. This is a state-of-the-art advanced numerical model that was originally developed at FFI during the late

1990s [2-4], and has continuously been improved since then. SISYFOS offers a set of software components corresponding to the optical components of a device. The core of the model is the component representing a nonlinear crystal. This module solves the coupled differential equations for the beams either by a split-step method or directly in (temporal and spatial) frequency-space. Both methods allow all relevant physical effects in the nonlinear crystal to be included:

- Arbitrary beam and pulse shape
- Propagation effects
    - Diffraction
    - Dispersion (temporal walk-off and pulse spreading)
    - Absorption
    - Birefringence (spatial walk-off)
- Second order nonlinearity
    - Phase matching
    - Pump depletion
    - Multiple mixing processes, e.g. parasitic processes
    - Birefringent phase matching
    - Quasi phase matching
    - Degenerate or non-degenerate interactions
- Nonlinear refractive index
    - Self-focusing
    - Self-phase modulation
- Two-photon absorption
- Thermal effects
    - Thermal lens
    - Thermal phase mismatch
- Quantum noise
- Highly non-collinear beams

In combination with the other components of the model a large class of devices can be represented:

- Non-resonant devices
- Ring or linear resonators
- Singly or multiply resonant devices
- Devices with multiple crystals
- Time scales from ultrafast to continuous wave
- Lasers

The model also allows inclusion of realistic problems such as

- Misalignment
- Non-ideal mirrors
- Absorption in components

The implementation is object oriented, with objects representing optical components or idealized components such as a beam source. The basic simulation code is written in C, the model defined by the user is built up and compiled in C++, and the user interface in Python. Matlab or Python can be used to analyze the results.

2.2 Pump beam

The beam from the 1064 nm Nd:YAG pump laser resembles an apodized top-hat distribution. For simplicity, we have assumed a circular symmetric super-Gaussian pump beam profile in most of the simulations. The intensity distribution of a super-Gaussian beam of order n with cylindrical symmetry follows the formula

$$I_n(r) = \frac{2^{\frac{2}{n}}}{\pi\omega^2\Gamma\left(1+\frac{2}{n}\right)} e^{-2\left(\frac{r}{\omega}\right)^n}, n = 2,4,6,... \qquad (2.1)$$

where ω is the half width at the $1/e^2$ point and Γ is the Euler-gamma function. In Figure 2.1, I is shown for n = 2, 4, 6 and 8. Also shown is the peak fluence of a 100 mJ beam for different beam diameters. To account for statistical variations in the transverse profile of the pump beam, we recommend using a $\geq$ 4 mm diameter beam at these energy levels to keep the pump fluence close to 1 J/cm^2. This can be considered to be a fairly conservative design criterion for 5-10 ns pulses, the surface damage threshold is for instance reported to be ~5 J/cm^2 in BBO [5].

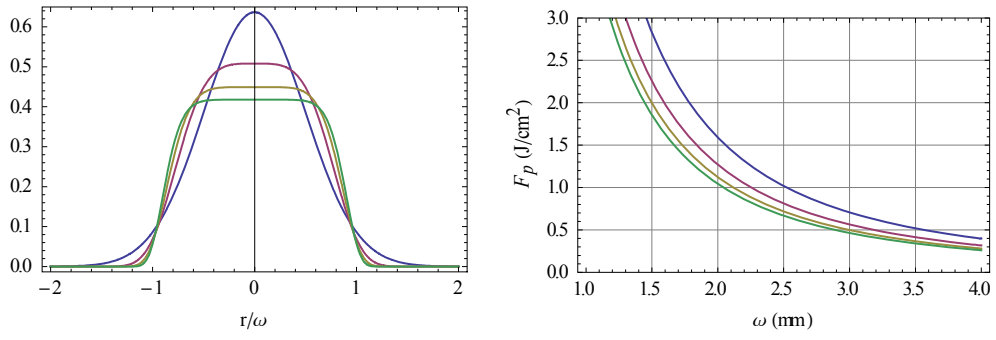

Figure 2.1 Left: Comparison of super-Gaussian distributions of order 2, 4, 6, and 8 (top and down at x = 0). Right: Calculated peak fluence as function of beam radius (ω) for a 100 mJ beam for circular symmetric super-Gaussian distributions of order 2, 4, 6 and 8 (top and down)

3 Considerations in the simulations

The performance of the nonlinear conversion stage is evaluated in terms of a few parameters of the output beam. These include total output energy, conversion efficiency, and beam quality. Among the parameters that need to be chosen and, if possible, optimized in an OPO or SFG device are nonlinear crystal and phase matching type, crystal length, beam size and, in the case of an OPO, mirror reflectivities and resonator geometry. In this chapter, the consequences of different choices for these parameters are discussed.

3.1 Parameters that can be varied

3.1.1 Nonlinear material and phase matching type

The most important choice in a nonlinear device is perhaps which crystal and which type of phase matching (PM) to use. Different nonlinear crystals that may be used in this work were reviewed in a previous report [1]. The polarization of a beam can be rotated with a half-wave plate, but this ads complexity to the set-up. If rotation of beam polarizations is to be avoided, it is clear that the SFG stage of both path 1 and 2 in Chapter 1 should be of type 2 PM since the polarization of the 1064 nm or 532 nm pump beam and the OPO signal beam will be orthogonal[1]. One advantage of type 2 PM that will be emphasized later in this work, is that the acceptance angle for the generated beams is smaller, thus making it possible to obtain a better beam quality in an OPO. It may therefore be preferable to apply type 2 PM even for the OPO stage. For the SFG-stage, on the other hand, the narrow acceptance angles may limit the conversion efficiency if the beam qualities of the pump and/or signal beams are too low. In this case, type 1 PM may be required.

3.1.2 Crystal length

A longer crystal gives a longer interaction length and better conversion efficiency, but if it is too long, the nonlinear process can be reversed. This *back conversion process* is important as it limits both conversion efficiency and beam quality, and it is central in the simulations to design a conversion stage where back conversion is avoided or, at least, weak. The optimal crystal length is also affected by the effective nonlinearity of the material as the small signal gain of the nonlinear interaction is a function of the product $d_{eff}L$, thus a smaller d_{eff} calls for a longer crystal. Additionally, the small signal gain also depends linearly on the signal frequency. Hence, if the crystals are similar, the lower frequency signal in a 1 µm pumped OPO requires longer crystals than the higher frequency signal in a 532 nm pumped OPO.

3.1.3 Beam diameter

Similar considerations are also made for beam diameters – smaller is usually better to a certain limit, below which back conversion occurs. There are also several other considerations that affect this choice. The angular spectrum of a beam becomes larger as the beam becomes narrower, resulting in increased divergence. Thus if the beam diameter is too small, its divergence may

[1] If type 3 PM is used in the OPO, this is not true, but the review [1] did not reveal any materials where this was a usable option. As will be discussed later, non-critical phase matching is not usable because the beam quality of the signal will be too poor

become substantial through the interaction length. As a rule of thumb, the beam's Rayleigh length should not be shorter than the crystal length. Additionally, if the angular spectrum of the beam becomes larger than the angular acceptance bandwidth of the nonlinear interaction, conversion efficiency will go down[2]. These two approximate restraints on the beam size can be expressed as:

$$\begin{aligned} &(1)\quad \omega_0 \geq \sqrt{\frac{L\lambda M^2}{\pi n}} \quad \text{(Rayleigh criterion)} \\ &(2)\quad \omega_0 \geq \frac{2L\lambda M^2}{\pi n \left| L\Delta\theta \right|} \quad \text{(Nonlinear interaction)} \end{aligned} \tag{3.1}$$

where ω_0 is the beam radius, L is the crystal length, M^2 is the beam quality factor, n is the index of refraction of the nonlinear material, and $L\Delta\theta$ is the angular acceptance interval for the nonlinear process [1]. For an $M^2 = 1$ beam at 532 nm wavelength in a 10 mm long KTA crystal, these limits become 30 μm and 320 μm, respectively.

If the combined fluence of the interacting beams becomes too large, optical damage may occur. This gives another power dependent limit to the beam size. The peak fluence of a super-Gaussian beam of order SG and energy E is $2k_{SG}E/\pi\omega^2$, where $k_{SG} = 2^{\frac{2}{SG}-1} \Big/ \Gamma\left(1+\frac{2}{SG}\right)$ is 1 for an order 2 function and 0.7 for an order 6 function (SG=6). Thus, the limit of the beam size is

$$(3)\quad \omega \geq \sqrt{\frac{2k_{SG}E}{\pi F_{\max}}} \tag{3.2}$$

where $F_{\max}$ is the maximum permissible fluence (typically on the order of 1-5 J/cm^2). For a 10 mJ beam, the beam radius should thus be above 0.8 mm if the maximum fluence is 1 J/cm^2. It should be noted that in (3.2), E should include all forward and backward propagating fields. Thus in resonators with low signal output coupling and double pass pumping, the required beam radius may be significantly larger than predicted by (3.2) based on the input pump beam alone. The total peak fluence is one of the results from the simulations. It should be noted that for the energy levels studied in this work, the limit given in (3.2) is the determining one as it will be much larger than the limits in (3.1).

The Fresnel number of a resonator is $a^2/\lambda L$, where L is the length of the resonator, λ is the wavelength, and a is a limiting radius in the resonator – in our case typically the pump beam radius. The larger this number is, the more higher-order transverse modes the resonator can sustain, and consequently, the poorer the beam quality of the oscillating beam(s). Recently, we found [6] that for an OPO with flat mirrors pumped by a pulsed beam with pulse lengths in the nanosecond range, the gain and the resonator provide sufficient spatial filtering to obtain good beam quality if the resonator Fresnel number, F, is less than or approximately equal to the number of round-trips in the OPO resonator during the pump pulse, N_{rt},

[2] This only applies in the direction of critical phase matching in the nonlinear crystal.

$$\frac{F}{N_{rt}} = \frac{\omega^2/\lambda L}{\tau_p c/2L} \leq 1 \quad \Rightarrow \quad (4) \quad \omega \leq \sqrt{\frac{\tau_p c \lambda}{2}} \ . \tag{3.3}$$

Here, ω is the pump beam radius, τ_p is the pump pulse length and λ is the signal wavelength. This result is somewhat surprising because it shows that it is possible to obtain good beam quality with significantly larger beams than the previous rule of thumb ($F \leq 1$). The cumulative spatial filtering described by this formula can be understood if one considers the first signal photons generated in the OPO. To be sufficiently amplified, these must overlap the pump pulse during a significant part of the pump pulse, hence the cumulative effect. Interestingly, the mirror spacing, L, is not a part of this expression because the increased spatial filtering a longer resonator offers is cancelled out by fewer round-trips during the pump pulse and thereby a smaller cumulative effect. It should, however, be noted that the resonator length is important for the conversion efficiency, and the resonator should therefore be made as short as possible.

Combining the optical damage limit (3.2) and the good beam quality limit (3.3), an approximation for the maximum pump energy in an OPO with good beam quality can be expressed as

$$E_{\max} \approx \frac{\pi}{4k_{SG}} \tau_p c \lambda F_{\max} , \tag{3.4}$$

where $F_{\max}$ here is the maximum permitted pump fluence, and the '≈' sign points out that this is an approximate expression. In this work, we consider OPOs with signal wavelengths of 650 nm and 1600 nm, while the pump pulse length is about 5 ns. Using (3.3), we find that good beam quality can be obtained from a standard OPO provided that the pump beam radius is less than 0.7 mm for the 650 nm OPO and 1 mm for the 1600 nm OPO. If the pump fluence is limited to 1 J/cm^2, (3.4) gives us that for a Gaussian beam the maximum pump energy for such OPOs would be 7.5 mJ for the 650 nm OPO and 18 mJ for the 1600 nm OPO. For order 6 super-Gaussian beams, the energies can be ~30% higher. However, as we aim for even higher output and hence pump energies in this work, it is clear that other means must be used to obtain sufficient beam quality.

3.1.4 OPO mirror reflectivities

In an OPO, the reflectivities at the three interacting wavelengths have great influence on the performance of the OPO. The simplified discussion below is for a linear two mirror resonator, but can also be expanded to other resonator geometries.

The input mirror of the OPO (where the pump beam is coupled into the resonator) should have high transmission at the pump wavelength. The output mirror could transmit the pump light or reflect it. The two alternatives are referred to as single-pass pump and double-pass pump, respectively. The latter approach has potential for higher conversion efficiency, but an optical isolator is normally required between the pump source and the OPO to prevent undepleted pump light to interfere with and potentially harm the pump source. The OPO intracavity fluence will be higher with such geometry, increasing the risk for optical damage. Also, the double-pass

approach makes use of the undepleted pump light in subsequent conversion stages difficult. Often, however, a double-pass pump is required to obtain useful conversion efficiencies, as will be seen later in this work.

The OPO resonator can further oscillate on one or both generated signals, usually referred to as singly resonant OPO (SRO) or doubly-resonant OPO (DRO), respectively. A DRO has a significantly lower threshold of operation than a SRO, but can be very sensitive to variations in the relative phase of the interacting beams [7]. Therefore, for practical devices, SRO is usually required. It is, however, often difficult to obtain truly SRO operation as the mirrors often have some reflection on the non-resonant beam. This may then affect the stability of an SRO.

The output coupler reflectivity on the signal wavelength is a compromise between a fast build-up time (low pump threshold), back-conversion and conversion efficiency, intracavity fluence, and OPO pulse length. The simulations later in this work will study the effects of different output couplings in detail.

3.1.5 Resonator geometry

In addition to mirror reflectivities, also the geometrical layout of the OPO resonator can have great influence on OPO performance. The most important alternatives are listed below.

The resonator can be linear or ring shaped. A linear resonator is simple to align, and the resonator roundtrip time can be made short, thus reducing the OPO build-up time and increasing the conversion efficiency. Often, a linear resonator requires an optical isolator between the pump source and the OPO to prevent unwanted reflections from the OPO to the pump source. This is not required with a ring resonator. Also, the intracavity fluence is lower in a ring resonator than in a linear resonator because one or more beams propagate both directions in the resonator in the latter. The round-trip time of the ring resonator is normally longer than for the linear resonator because the air gaps between the crystals and the mirrors must be made longer. This may result in lower conversion efficiency, in particular for pumping with short (a few ns) pulses. While the linear resonator requires two mirrors, the ring resonator normally require three or four mirrors, making it considerably more difficult to align and optimise. On the other hand, more mirrors also provide an opportunity to for example remove the idler at several positions in the resonator [8], which may reduce back-conversion and improve the performance. Both linear and ring resonators will be studied later in this work.

The resonators can also be made stable or unstable by a careful selection of radius of curvature of the mirrors and the position of the mirrors. There are reports that unstable resonators have resulted in improved beam quality from OPOs, but often at the expense of a poorer conversion efficiency [9-11], and this will to some extent be investigated in the simulations. In reality, even unstable resonators may de facto be stable because of the strong gain guiding of the nonlinear process, but because this depends on the intensities of the interacting beams, this will vary through the pulse and is difficult to estimate. The most common resonator in the simulations (and in most published work) consists of flat mirrors.

Instead of using a simple OPO stage, a master oscillator – power amplifier (MOPA) geometry can also be used. Here, the requirements of high beam quality and high conversion efficiency can be split since the beam quality from an OPA stage to a large content depends on the quality of the input beams [12]. Thus, a low power master oscillator with high beam quality can be designed, for which efficiency is not a major issue, and the beam from this stage can be amplified in an OPA which is optimized for high conversion efficiency. A major draw-back with a MOPA approach is the considerably added complexity to the setup with more crystals and beam paths. It is, for example, important that the laser pump pulse and the pulse from the master oscillator overlap in time in the OPA. This requires careful design of beam lines and may require beam delay lines. It is advantageous to maintain the top-hat-ish profile of the near-field of the pump laser throughout the MOPA system, but as the beam profile of the pump beam changes considerably over a distance of ~100 cm the propagation distances may become too large. In this case, the beam must be relay imaged from the laser onto the nonlinear crystal. Relay imaging includes two lenses and an intermediate focus, and since the pump energy is high, the focus should be inside a vacuum tube to avoid sparkover, which will occur in air. The MOPA geometry will, when properly designed, work well under many circumstances, but the much added complexity of the experimental lay-out make it our choice only if satisfactory performance cannot be obtained from an OPO directly.

3.2 Challenges in obtaining high conversion efficiency

A main challenge in designing efficient OPOs that are pumped with nanosecond pulses is the large and rapid variation in pump intensity. In an OPO the build-up time of the generated light may be a substantial fraction of the pump pulse length, thus greatly reducing the efficiency. On the other hand, if the OPO is optimized for high gain at the low pump intensities at the leading edge of the pump pulse, then significant back conversion may occur at peak pump intensity. There is also a great transverse variation in the intensity across the pump beam profile which should be accounted for. In the case of a multi-longitudinal mode pump, a very fast and random modulation of the pump intensity makes in many cases the conversion efficiency smaller [13]. All these processes need to be accounted for in simulations of the nonlinear conversion stage for a reliable simulation of the system.

3.3 Beam quality

3.3.1 Required beam quality

The beam quality, M^2, of a laser beam is a description of how much a beam of a certain beam diameter diverges compared to that of an ideal beam. In remote sensing applications, it is important that the divergence is smaller than the field of view of the detection system. For example, the detection channel in FFI's biolidar [14] consists of a 1200 mm focal length telescope that focuses the light onto a 365 μm diameter optical fiber, resulting in a 0.3 mrad field of view (FOV). The full far field divergence angle of the laser beam is given by

$$\theta = 2M^2 \frac{\omega_0}{z_R} \tag{3.5}$$

where ω_0 is the beam waist radius and z_R is the Rayleigh length of the beam ($z_R = \pi\omega_0^2 / \lambda$).In Figure 3.1, the fraction of the UV laser beam energy that is within a 0.3 mrad FOV is shown as function of M^2 for different beam sizes assuming that the beam has a Gaussian transverse profile with a divergence according to (3.5). For this application, M^2 < 8-10 thus seems like a reasonable requirement. For 1 mrad FOV, the corresponding requirement would be M^2 < 25.

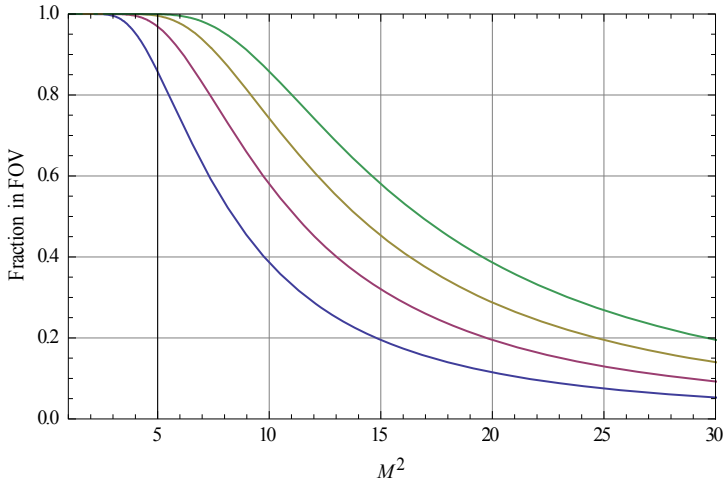

Figure 3.1 Fraction of a 290 nm beam that is within a 0.3 mrad FOV as function of beam quality for 3 mm, 4 mm, 5 mm and 6 mm beam waist radius (bottom to top)

3.3.2 Factors influencing on the beam quality

While it is an obvious target to have high beam quality in the generated beams both to be able to obtain high conversion efficiency in subsequent conversion stages and for efficient use of the final beam in remote sensing applications, there are several processes that have a detrimental effect on the beam quality of the generated laser beam. Factors that influence signal beam quality are

- Beam quality of pump beam(s)
- Resonator geometry (in OPOs)
- Back conversion
- Poynting vector walk-off

To some extent, the choice of nonlinear material and phase matching type may help improving the beam quality as a narrow acceptance angle and type 2 PM may significantly improve the beam quality in the direction of critical phase matching[3]. Thus, the beam quality of an OPO may be asymmetric since the angular acceptance bandwidth of the nonlinear interaction is very

[3] The direction of critical phase matching is the direction which can be angle tuned. The noncritical direction is normal to this and the direction of beam propagation

different in the direction of critical phase matching and the direction of noncritical phase matching. Later in this report, we will discuss methods to reduce asymmetry of the OPO beams.

Back conversion has a detrimental effect on the beam quality. Back conversion typically becomes important when the generated field strengths become comparable to the pump field. It is important in the design of the nonlinear conversion stage to reduce this process, which can be done by a proper choice of crystal length, beam diameter, and output reflectivities (for the OPO). Poynting vector walk off causes beams of different polarization to propagate at slightly different angles in a birefringent crystal. The walk-off angle is typically in the 1-5º range for the materials and processes in question in this work [1]. If the walk-off distance through the nonlinear material is comparable to the beam diameters, walk-off will reduce conversion efficiency as it limits the interaction distance in the nonlinear crystal. Hence, the beams should not be narrower and the crystal not longer than what makes the walk-off distance through the material smaller than the beam diameter,

$$\alpha_{WO} L < 2\omega \tag{3.6}$$

where α_{WO} is the walk-off angle. For a 10 mm KTA crystal, the beam diameter should then be > 580 µm. Contrary to what one may think, walk-off between signal and idler, as is the case in type 2 PM, may actually lead to an improved beam quality in the direction of walk-off [15]. This will be discussed in more detail in the next section.

3.4 Techniques to improve performance

The often conflicting requirements for design of the nonlinear conversion stage make optimization of the architecture difficult. There are, however, several techniques that can be used that improve the performance substantially. The most important ones are listed in this section.

3.4.1 Pump beam quality

Armstrong and Smith [13, 16] have shown that the beam quality of the pump beam is important for the performance of the nonlinear conversion stage, and they spent considerable effort in improving the pump beam quality. This is, however, outside the scope of this work.

3.4.2 Length matching

The performance of an OPO that is pumped by an MLM (multi-longitudinal mode) beam can be improved if the length of the OPO resonator is matched to that of the pump laser [17, 18]. However, as the performance of the OPO generally is reduced for longer resonators because of increased build-up time, this optimization is only useful if the laser resonator is short and comparable in length to the minimum OPO length. The pump lasers that can be used in this work, typically has resonator roundtrip lengths on the order of 50 cm whereas typical minimum OPO resonator lengths are on the order of 10 cm. Therefore, length matching will not be considered here.

3.4.3 Walk-off compensation

Poynting vector walk-off reduces the maximum interaction distance in a nonlinear crystal, and hence conversion efficiency. If a longer interaction length than allowed by Eq. (3.5) is required, this can be accomplished by using two crystals in a *walk-off compensating geometry* [19]. Here, the second crystal is oriented such that the direction of walk-off is reversed, in part cancelling the effect. By using several pairs of walk-off compensated crystals, the total interaction length can be made significantly longer than is possible within one crystal. The drawback of this technique is more optical surfaces that can be damaged or contribute to loss, and an added complexity to the system, in particular if angle tuning of the crystals is required. As the beam sizes in this work typically are much larger than given by (3.6), walk-off compensating geometries will only be considered for the small beam sizes in a low energy master oscillator here.

3.4.4 Reducing back conversion

Back conversion of the generated beam(s) to the original beam(s) has detrimental effect on the performance of a nonlinear conversion stage. Back conversion occurs when the generated beams have grown to a certain intensity level while still in the nonlinear crystal. Back conversion can be reduced by carefully selecting the length of the nonlinear crystal, but in an OPA/OPO process, it can also be reduced by splitting the crystal into two or more shorter crystals and removing one of the generated beams (in most cases the idler) between the crystals with a filter or a mirror [8, 12]. Such means for improving the performance will be examined in the simulations described here. In some nonlinear materials, like BBO, there is significant absorption at wavelengths longer than 2.5 μm. The OPO idler wavelength is in this range for both architectures studied here. This idler absorption may help improve the performance of the OPO for low pulse rates as it reduces back conversion. For high pulse rates, the heat load from idler absorption leads to thermal lensing that will cancel the improving effect. The pulse rate at which this occurs depends on the beam size, absorbed energy and parameters of the nonlinear material, but is typically in the 10-1000 Hz range [6].

3.4.5 Improving beam quality

Reducing the beam radii may improve the beam quality in an OPO since fewer transverse modes can be sustained within the gain area. The minimum beam size is however limited by the requirements in (3.1-3) and (3.6). In theory, it is possible to design a stable resonator such that the fundamental mode radius is large and, consequently, the higher order modes are even larger. However, as gain guiding in the nonlinear material is the most important stabilizing element in the resonator and since the exact magnitude of this is varying through the pulse and hence difficult to predict, this is probably not a good alternative. Additionally, stable resonators with large beam diameters often have long resonator lengths, which is bad for obtaining high conversion efficiency from nanosecond OPOs. Another approach is to design unstable resonators such that the higher order modes have higher losses, as was briefly described earlier in this report. The beam quality can also be improved at the expense of simplicity with a master oscillator – power amplifier (MOPA) geometry, as described above. Both different OPO resonator geometries and MOPA geometries will be studied in the simulations.

3.4.6 Reducing asymmetry in beam quality

Type 2 phase matched OPOs with large beams and short resonators tend to have a highly asymmetric beam quality. The reason for this is that the nonlinear material in the OPO is a highly selective filter in the direction of critical phase matching, while it is less selective in the other, non-critical direction. This is in particular true for type 2 PM where the two generated beams have different polarizations, and hence have walk-off from each other. Walk-off makes the phase and amplitude of different transverse parts of the signal and idler beams correlated, resulting in a relatively flat phase front of the generated beams in the direction of walk-off. In the direction perpendicular to the walk-off direction, the beams are generally less correlated and, hence, have poorer beam qualities [15].

There are different approaches that may reduce this asymmetry. Using beams with elliptic cross-section where the narrow dimension is in the non-critical direction will improve the beam quality in this direction at the expense of the beam quality in the other direction. This approach may require very large crystals in one direction, and the maximum available apertures may limit the usefulness of the approach. It will be briefly examined in the simulations. Another method may be to use unstable resonators that have a larger magnification (=loss) in the noncritical direction than in the direction of critical phase matching. This will also be studied.

A few alternative approaches to reduce the asymmetry by rotation of the image of the beam, but not its polarization have been demonstrated in the literature. The basic idea is to use the beam quality improvement in the critical direction in both directions of the beam. Nabors and Frangineas [20] used non-collinear phase matching in both directions and a Porro prism in the non-critical direction in a type 1 phase matched singly resonant BBO OPO with double pass pump and obtained a factor of ~10 improvement in beam quality compared to a standard resonator, but the bandwidth of the OPO increased significantly. Anstett *et al.* [21] used a retro-prism and a half-wave plate in a type 2 phase matched singly resonant BBO OPO with double pass-pump, and obtained a narrow spectral and spatial beam. Pasiskevicius *et al*. [22] found the beam quality of an OPO based on periodically poled KTP to improve with non-collinear phase matching. Smith *et al.* [15, 16] developed a ring resonator geometry in which the resonated beam is rotated 90 degrees with a Dove prism (or a similar mirror arrangement) while the polarization is unchanged thanks to two half-wave plates. The beam quality obtained was symmetrical, and the conversion efficiency was high. In this work, much effort was also put into improving the beam quality of the pump laser.

3.4.7 A new approach for reducing asymmetry in beam quality

Although approaches described in the previous section can improve beam quality and reduce asymmetry, they all include complex experimental designs. We have developed a different approach that also can solve the problem with asymmetric beam quality. This is accomplished by using crystals with different critical planes and hence walk-off directions in the same OPO.

In a type 2 phase matched OPO, the signal beam will always be polarized in the slow direction (i.e. the direction of highest refractive index), while beams with polarization in the direction of

the extraordinary index has walk-off. In some materials, these directions are parallel (positive materials) while in other materials they are orthogonal. For example, in the negative uniaxial crystal BBO, the slow axis is the ordinary axis, while for phase matching the XZ-plane in the biaxial crystal KTA, the slow axis is the extraordinary axis (for propagation angles greater than 17º (optics axis) with the Z-axis). The crystal plane for critical phase matching includes the extraordinary axis and the direction of propagation, and walk-off is in this plane. Hence, as the critical planes are orthogonal in BBO and KTA for the same set of beams, the walk-off directions will also be orthogonal, as is illustrated in Figure 3.2. In Table 3.1, an overview of potential materials and their walk-off and type 2 PM properties is given for a 532 nm pumped OPO, and similar data for a 1064 nm pumped OPO are given in Table 3.2.

The ideal material for this OPO should have both a high nonlinearity and a large walk-off angle (because this leads to a small acceptance angle). For the materials with slow axis walk-off, both KTP and KTA (and probably its isomorphs) are good choices. In the simulations later in this work, we have used KTA, but as KTP has very similar properties to KTA, it can be expected that similar results can be obtained with KTP. For the materials with fast axis walk-off, there is less to choose from. The best choice appears to be BBO although this material has significant idler absorption. Recently, we showed that such absorption may improve the performance of low pulse rate OPOs as it helps reduce back conversion [6].

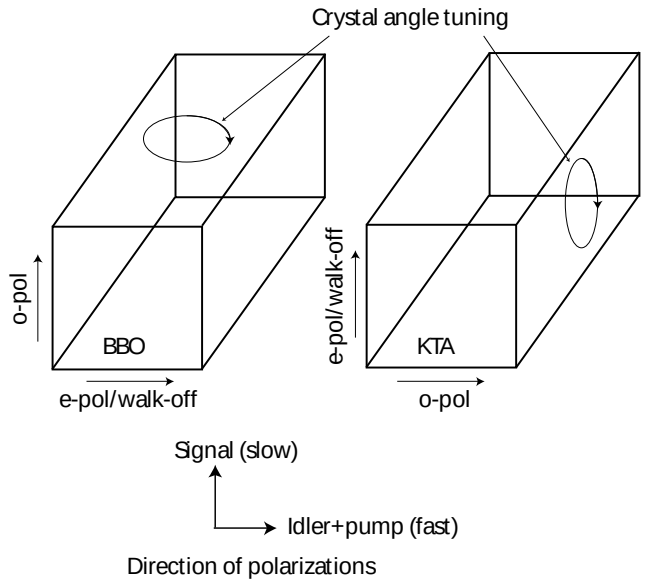

Figure 3.2 Sketch of axes and walk-off directions for negative and positive crystals for type 2 PM

Material	S/F wo	U/B	θ/φ º	d_{eff} pm/V	$L\Delta\theta_2$ mm·mrad	WO º	Ref
KTP	Slow (XZ)	B (19º)	43/0	2.7	5.6	3.1	[23, 24]
KTA	Slow (XZ)	B (17º)	43/0	2.0	5.9	3.0	[23, 25]
BBO	Fast	U	23	1.4	5.6	2.9	[23, 26]
BiBO	Slow (XZ)	B (26º)	40/0	1.8	3.5	5.2	[27, 28]
YCOB	Fast (XY)	B (61º)	90/30	1.1/1.3*	34.0	0.9	[29, 30]
LNO	Fast	U	54	0.7	5.9	2.4	[31, 32]
LBO	Fast (XZ)	B (54º)	30/0	0.3	33.6	1.3	[32, 33]
KDP	Fast	U	45	0.39	12.2	1.6	[34, 35]

*) Depends on the sign of d_{31} which varies in the literature

Table 3.1 Materials for type 2 PM OPO for 532 nm → 650 nm conversion. "S/F wo" lists whether slow or fast axis has walk-off, U/B lists whether the material is uniaxial or biaxial, and the angle of the optics axis in the latter case, $L\Delta\theta_2$ is the acceptance angle for the signal (calculated from non-collinear PM, see Appendix B), and WO is the walk-off angle

Material	S/F wo	U/B	θ/φ º	d_{eff} pm/V	$L\Delta\theta_2$ mm·mrad	WO º	Ref
KTP	Slow (XZ)	B (18º)	46/0	2.1	16.2	2.8	[23, 24]
KTA	Slow (XZ)	B (17º)	42/0	1.9	17.4	2.6	[23, 25]
BBO	Fast	U	29	1.4	11.9	3.6	[23, 26]
BiBO	Slow (XZ)	B (26º)	42/0	1.9	9.4	4.9	[27, 28]
YCOB	Fast (XY)	B (61º)	90/41	0.8/1.1*	76	0.9	[29, 30]
LNO	Fast	U	56	0.65	15.7	2.4	[31, 32]
LBO	Slow (YZ)	B (54º)	42/90	0.5	96	0.5	[32, 33]
$AgGaS_2$	Fast	U	74	12	51	0.7	[36, 37]

*) Depends on the sign of d_{31} which varies in the literature

Table 3.2 Materials for type 2 PM OPO for 1064 nm → 1650 nm conversion. The columns are explained under Table 3.1

3.4.8 Improving conversion efficiency of the SFG stage

In this chapter, a number of different approaches to improve the performance of nonlinear conversion stages have been listed, in particular for the OPO. When it comes to improving the conversion efficiency of the total system, the conversion efficiency of the final SFG stage is also important. The efficiency of this stage depends on the beam quality and the spectral bandwidth of the incident beams, the spatial and temporal overlap, as well as crystal length and beam sizes. It is important to examine the importance of these parameters in the simulations. For example, to obtain optimal temporal overlap between the pump pulse and the pulse from the OPO, a delay line is likely to be required. This increases the complexity of the system considerably, and may, if the delay line is long, even require relay imaging to preserve the top-hat profiles of the interacting beams. It would be clearly advantageous to avoid such arrangements.

3.5 Summary

A number of different topics to consider in the design of efficient nonlinear conversion stages have been listed in this chapter. Most of these topics will be considered in the following chapters

where simulations of the two schemes listed in Chapter 1 are presented. Particular attention will be on the new method for improving the beam quality described in section 3.4.7.

There are two main approaches to achieve the pulse energies necessary to pump the sum frequency stage. These will be studied in Chapter 4, both for 1064 nm and 532 nm pumping. The the sum frequency stage is studied in Chapter 5.

4 Generation of high energy at 650 nm and 1650 nm

4.1 General considerations

4.1.1 What is the optimum use of pump energy?

As the pump energy is used to pump two different nonlinear stages, finding the optimal distribution of the pump energy between those two stages is important for the overall efficiency. The SFG-process is a combination of two photons to create a new one. Therefore, optimally there should be equal numbers of photons in the two beams incident on the SFG stage provided that the beams overlap perfectly temporally and spatially. This corresponds to an energy ratio of the beams of $E_{650}/E_{532} = 0.82$ and $E_{1650}/E_{355} = 0.22$ for the two architectures studied in this work.

In the following analysis we number the beams in the SFG process as follows:

1. Longest wavelength (i.e. from OPO - ~650 nm or ~1650 nm)
2. Shortest pump wavelength (in this work 355 nm or 532 nm)
3. Generated wavelength (~290 nm)

We assume that the output energy from the OPO-stage can be written as

$$E_1 = \eta_1 \left(E_P - E_{th,1} \right) \tag{4.1}$$

where E_P is the pump energy pumping the OPO stage and $E_{th,1}$ is the threshold pump energy for the OPO, and that the energy in beam 2 can be written as

$$E_2 = \eta_2 \left(E_L - E_P - E_{th,2} \right) \tag{4.2}$$

where E_L is the total laser energy available, and $E_{th,2}$ and η_2 are the threshold pump energy and the efficiency in generating beam 2 in the SFG process, respectively. Requiring the number of photons of each beam ($N \sim \lambda E$) to be equal yields

$$r_{P,0} = \frac{E_P}{E_L} = \frac{1}{1 + \lambda_1 \eta_1 / \lambda_2 \eta_2} \left(1 - e_{t2} + \frac{\lambda_1 \eta_1}{\lambda_2 \eta_2} e_{t1} \right) \tag{4.3}$$

where λ_i is the wavelength of beam i and e_{ti} is the threshold of beam i relative to the total pump energy E_L. In Figure 4.1, this ratio is shown as function of OPO efficiency for the two approaches in this work. Here, 30% slope efficiency and zero threshold for 355 nm generation has been assumed, which is in reasonable accordance with the available pump laser. For the 532 nm pumped architecture, 100% slope and zero threshold are used since the distribution of 532 nm photons does not depend on the efficiency of the 1064 nm to 532 nm second harmonic process.

Three different values of the OPO threshold are shown in each case, corresponding to 0, 25 mJ and 50 mJ threshold in the two cases. Note that E_L in the left hand graphs refers to 532 nm pump energy, while it in the right hand graphs refers to 1064 nm pump energy. If we assume an OPO slope efficiency (as defined in (4.1)) of 30-40%, we observe that the 532 nm pumped OPO should be pumped with 70-80% of the available 532 nm pump energy, while the 1064 nm pumped OPO should be pumped with ~20% of the available 1064 nm pump energy, and that this value increases with increasing OPO threshold. Assuming that the available pump energy is 200 mJ and 600 mJ at 532 nm and 1064 nm, respectively, the recommended pump energy is 140-160 mJ at 532 nm and ~120 mJ at 1064 nm. This result is a first approximation and is modified for several reasons which will be dealt with below.

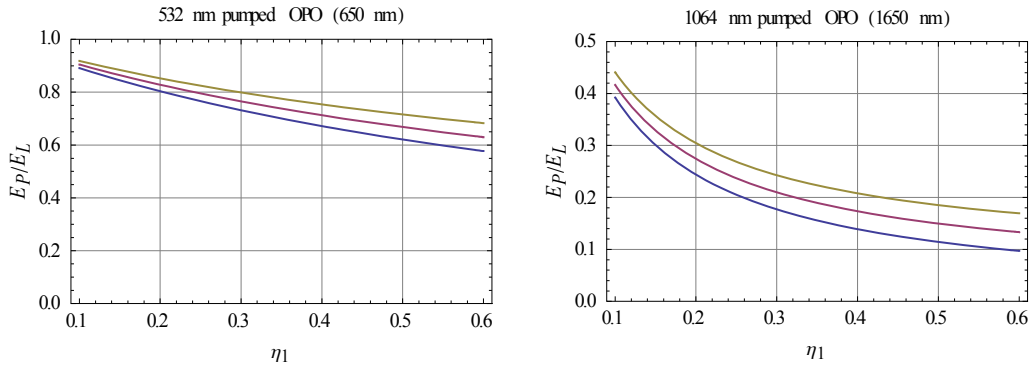

Figure 4.1 Optimal distribution of pump energy as function of OPO slope efficiency. Left: 532 nm pumped 650 nm OPO where e_{t1} is 0, 0.125 and 0.25 (bottom and up), corresponding to 0, 25 mJ and 50 mJ at 200 mJ available pump energy. Right: 1064 nm pumped 1650 nm OPO assuming 30% slope efficiency and 0 threshold for 355 nm generation for e_{t1} is 0, 0.04 and 0.08 (bottom and up), corresponding to 0, 25 mJ and 50 mJ at 600 mJ available pump energy

The calculations above are valid for perfect overlap between the beams. It is also of interest to examine the effect of imperfect overlap, and in particular the effect on the total efficiency when the photons in one of the beams are in excess. The total output energy from the SFG stage can be estimated by

$$E_3 = \eta_3 \left(E_1^* + E_2^* \right) \tag{4.4}$$

where the '*' denotes that the energy of the excess beam is reduced to have equal number of photons as the other beam. In the case of E_P less than the limit given by (4.3), there will be less photons in beam 1 than in beam 2. We thus find:

$$E_3 = \eta_3\left(\frac{N_1}{\lambda_1}+\frac{N_1}{\lambda_2}\right) = \eta_1\eta_3\frac{\lambda_1}{\lambda_3}\left(r_P - e_{t1}\right)E_L \ , \ r_P \le r_{P,0} \tag{4.5}$$

where $r_p = E_p/E_L$. Similarly, we find for E_P larger than given by (4.3)

$$E_3 = \eta_3\left(\frac{N_2}{\lambda_1}+\frac{N_2}{\lambda_2}\right) = \eta_2\eta_3\frac{\lambda_2}{\lambda_3}\left(1 - r_P - e_{t2}\right)E_L \ , \ r_P \ge r_{P,0} \tag{4.6}$$

In Figure 4.2, E_3/E_L is plotted as function of r_P for different η_1. In the calculations, e_{t1} = 0.25 and 0.08 for the 532 nm and 1064 nm pumped OPOs, respectively, and the SFG efficiency, η_3, is assumed to be 30%. It should be noted that the higher conversion efficiency of the 532 nm pumped system does not account for the conversion efficiency from 1064 nm to 532 nm. If this is included (η_2 ~ 30% in our laser which is optimized for 355 nm generation, but up to 60-70% available from systems optimized for 532 nm generation), the total systems perform comparably. We note, however, that the 532 nm pumped system is more affected by a change in the OPO efficiency, which is natural since a greater part of the pump energy is applied at this stage than for the 1650 nm OPO.

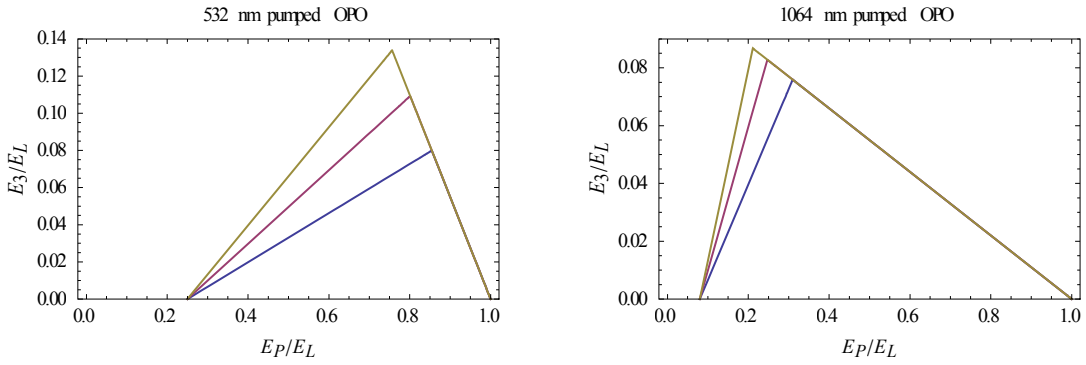

Figure 4.2 Estimated conversion efficiency to the UV as function of pump distribution for OPO slope efficiencies of 20%,30% and 40% (bottom and up) assuming 30% efficient 355 nm generation, and e_{t1} = 0.25 and 0.08 for the 532 nm and 1064 nm pumped OPOs, respectively

Finally, by comparing the slopes of a curve below and above the optimal point, we can see which photons are less costly in case a perfect balance between beams 1 and 2 cannot be obtained in the SFG process. In Figure 4.3, the absolute values of the derivatives of curves in Figure 4.2 are shown as function of η_1. We notice that for the 532 nm pumped OPO, it has less effect on the total performance if there is an excess of 532 nm photons (smaller r_P value), while for the

1064 nm pumped OPO, the OPO signal should rather be in excess on the SFG stage than the 355 nm beam.

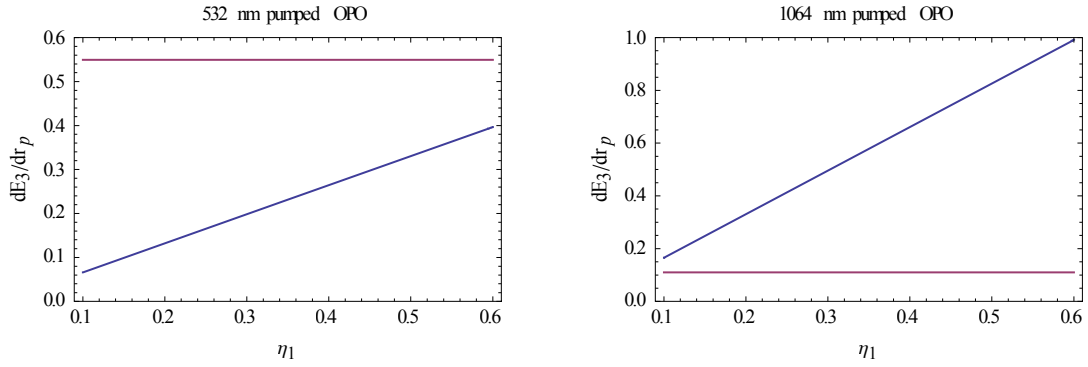

Figure 4.3 Absolute values of the derivative below (blue curves) and above (red curves) the optimal point in Fig. 4.2 as function of OPO efficiency. Lower values mean that the system efficiency is less affected by an adjustment of r_P in this direction. e_{t1} is taken to be 0.25 in the left graph and 0.08 in the right graph

Using these results and taking into account that the pulse lengths of the beams may be different, we can make some recommendations regarding distribution of pump energy between the OPO and SFG stages. The OPO pulse length is generally shorter than the pump pulse length, mainly owing to the build-up time of the OPO. Therefore, the ratio of the number of photons in the two beams will vary with time, as is shown in Figure 4.4.

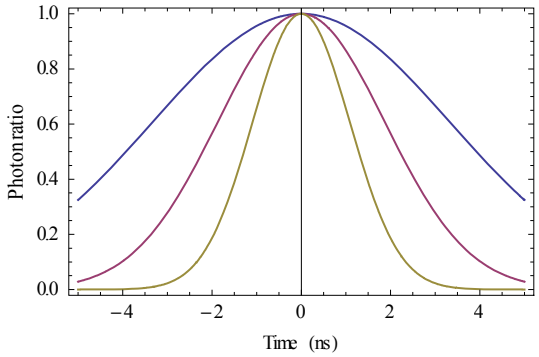

Figure 4.4 Ratio of photon densities between Gaussian pulses with 2 ns, 3 ns, and 4 ns FWHM pulse length (bottom to top) to a 5 ns pulse length assuming equal photon numbers at t = 0

For the 532 nm pumped stage, where it is better to have pump photons in excess, requiring equal number of photons at pulse peaks is a good estimate. The modified optimal energy distribution is shown in Figure 4.5 as function of OPO pulse length. We see that for 4 ns OPO pulse, ~60% of the 532 nm energy should be used to pump the OPO. This corresponds to ~120 mJ with the pump laser available to this work, and is also what is used in the simulations later in this chapter.

For the 1064 nm pumped OPO, the task is more complex. From Figure 4.3, it was clear that we should have 1650 nm photons in excess rather than the 355 nm photons. However, since the 1650 nm pulse generally is shorter than the 355 nm pulse, there will inevitably be some excess of 355 nm photons at the flanks of the pulse. A natural choice would then be to require equal number of photons at some point on the rising flank of the pulses – the challenge is to determine which point in time to use. In Figure 4.5, the optimal energy ratio is shown as function of point in time where the numbers of photons are required equal. We notice that if we require the number of photons to be equal at the half max value of the OPO signal (i.e. at 2 ns for a 4 ns FWHM OPO pulse), the optimal OPO pump energy is 20-25% of the pump energy, while for equal photon numbers at 3 ns, ~30% of the pump energy should be used to pump the OPO. As this analysis is by nature approximate, we leave for the detailed numerical simulations to examine this distribution further. In the simulations of the OPO, we have used 120 mJ pump energy, knowing that a moderate change in pump energy will not have a great effect on the design parameters of the OPO.

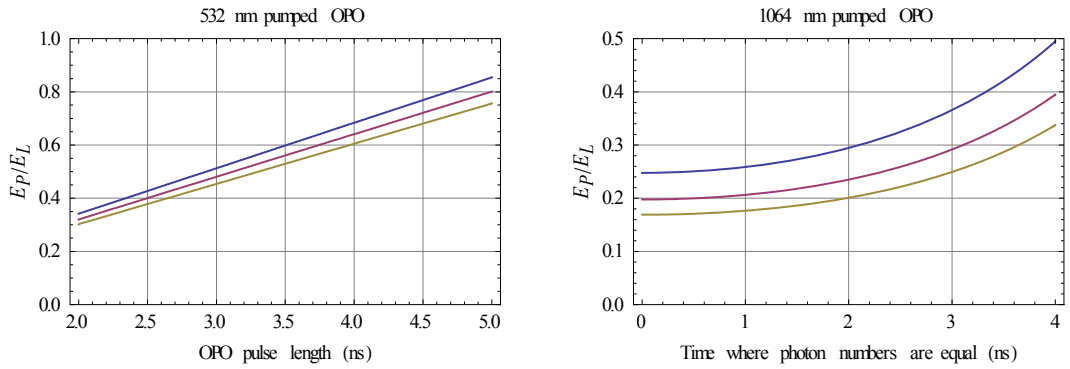

Figure 4.5 Optimal pump distribution accounting for differences in pulse lengths. Left: Optimal ratio as function of 650 nm OPO pulse length for a 5 ns 532 nm pump pulse length (FWHM) for 20%, 30% and 40% 532 nm OPO efficiency (top to bottom). Right: Optimal ratio for 4 ns 1650 nm OPO and 5 ns 1064 nm pump pulse lengths (FWHM) as function of time before peak where photon densities are equal for 20%, 30% and 40% OPO efficiency (top to bottom). e_{t1} is taken to be 0.25 in the left graph and 0.08 in the right graph

4.1.2 Resonator geometry

There are two main resonator geometries that can be applied in an OPO: A linear resonator or a ring resonator. In the linear resonator, the resonated wave travels back and forth between the end mirrors producing a standing-wave inside the resonator, while in the ring resonator the resonated wave travels around the resonator in the direction of the pump[4], as is sketched in Figure 4.6. There are cons and pros with both geometries and the most important of those are listed below.

A linear OPO is generally a simple geometry, and the resonator can be made very short as the mirrors can be placed close to the nonlinear crystals. It is easy to align experimentally, and has

[4] In a laser, even the ring resonator may be a standing wave resonator, but for OPOs the generated beams are only amplified when travelling along with the pump wave, hence single direction operation is ensured

potential for high conversion efficiency. The conversion efficiency can also be improved by using double pass pump, i.e. reflecting the undepleted pump at the output coupler. This will require an optical isolator between the pump source and the OPO to avoid instabilities as well as optical damage on the pump source caused by feedback to the pump source. Draw-backs with a linear resonator are that a short resonator and a wide pump beam may lead to a poor beam quality, and that the intracavity fluence may be high. The ring OPO on the other hand does not require an optical isolator, but is considerably more challenging to align. More mirrors are required, and in some cases also more crystals (compared to the linear resonator with double-pass pump). The folding mirrors require more space than the mirrors in the linear resonator, making the resonator round trip time longer than for the linear resonator (see Fig. 4.6c). However, compared to a linear resonator with single-pass pump, the absence of material in the return pass (Fig. 4.6b) may actually make the resonator round-trip time shorter for the ring resonator than for the linear resonator, thus improving the conversion efficiency. Also, the added air-gaps in the ring resonator may improve the beam quality compared to the linear resonator.

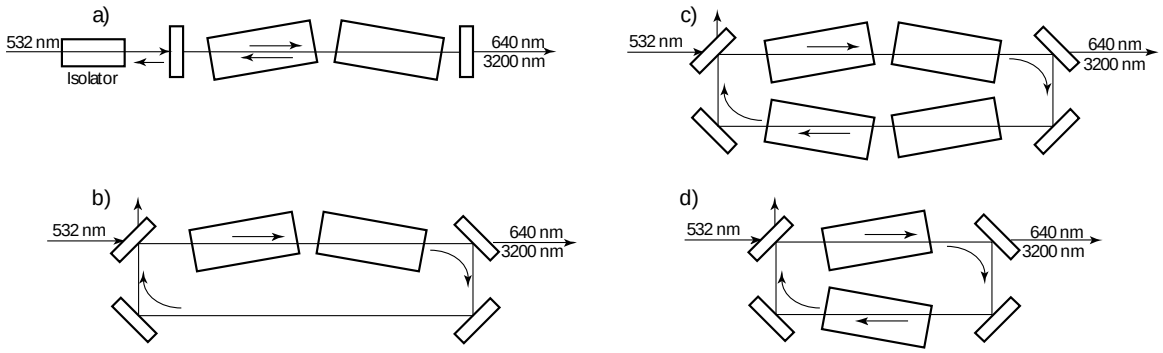

Figure 4.6 Schematic of linear and ring resonator geometries for OPOs indicating position of mirrors and nonlinear crystals. Arrows indicate direction of propagation. In this example pair(s) of walk-off compensating nonlinear optical crystals (see Sect 3.4) has been assumed. Ring b) compares to a) with single-pass pump, while ring c) compares to a) with double-pass pump. Ring d) is comparable to b), but with output coupling between the crystals

There are different ways to experimentally realize both linear and ring resonators. One example is shown in Figure 4.6d where the second nonlinear crystal is placed in the second arm of the ring, otherwise being nearly identical to the ring in Fig. 4.6b, except that the signal output coupling occurs between the crystals. In Figure 4.7, the different resonators are compared with two or, in the case of geometry c), four 20 mm long KTA crystals and 50% reflectivity on the resonated signal beam pumped at 532 nm. In the simulations, the pump beam diameter was assumed to be 6 mm for the linear resonator with double pass pump, while for the other geometries, the pump beam diameter was set to 4.4 mm. The reason for this is that the total fluence in the linear resonator is higher than in the other geometries owing to the presence of the pump in both directions. In all simulations, the peak total fluence was ~2 J/cm^2. We observe that the geometries with longest gain length in the resonator perform better than the other geometries, with ring c slightly better than the linear geometry with double pass pump. The beam quality from the ring

geometries was slightly better than the linear geometries, but the beam was still highly asymmetric (M^2 ~ 2 x 9 vs. 2 x 14). As the ring performs only marginally better than the linear geometry at the expense of experimental complexity and crystal cost, we choose to proceed with the linear resonator with double pass pump in the rest of this work.

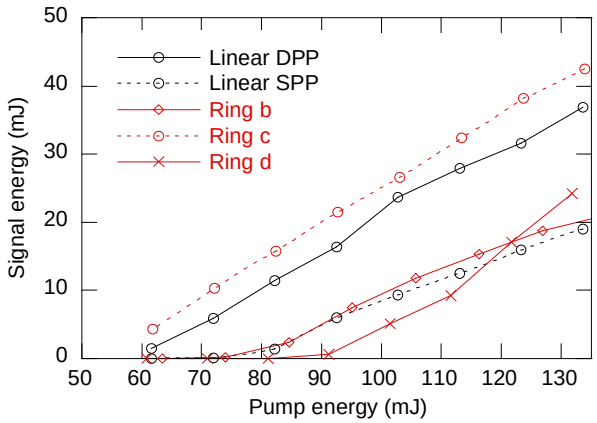

Figure 4.7 Summary of 532 nm based OPO simulations with different resonator geometries. SPP = single-pass pump, DPP = double-pass pump, ring b, c or d refer to the corresponding geometry in Fig. 4.6

We note that ring d performs differently from ring b in Figure 4.7. The reason for this is that the position of the output coupler reduces the intensity of the signal and idler beams in the second crystal in ring d. This reduces the performance of the OPO near threshold, but reduces back conversion at high pump energies, as can be seen in Figure 4.7.

4.1.3 Choice of nonlinear material

The small signal gain of an OPO depends on the product $d_{eff} \cdot L_{crys}$, thus a lower nonlinear gain can, to some extent, be compensated for by a longer crystal. Other important parameters are absorption losses at all three wavelengths, optical damage threshold, heat handling capabilities, as well as commercial availability and other material properties like hygroscopic/non-hygroscopic and ruggedness. In [1] we found KTA to be the best choice for type 2 phase matched 532 nm and 1064 nm pumped OPOs, with KTP as an alternative choice. KTA and KTP have similar parameters, but KTA was recommended because of its significantly higher transmission at the idler wavelength around 3 µm.

In the hybrid OPO as was described in Section 3.4.7, we have chosen BBO as the second material. Of the alternatives listed in Tables 3.1-2, it offers the best combination of d_{eff} and walk-off angle. IR transmission in BBO is limited, but – as shall be seen in the simulations, this does not reduce the performance of the OPO significantly.

4.1.4 Reducing beam asymmetry

The output from a high pulse energy KTA-based OPO is highly asymmetric, as is shown in Figure 4.8 below. We notice that although the near field appears to be fairly symmetrical, there is

a large difference in the far field divergence in the direction parallel to and perpendicular to the direction of walk-off. In Sections 3.4.6-7, we have listed some methods that may help reducing this asymmetry. In the following sections, simulations applying these techniques are presented.

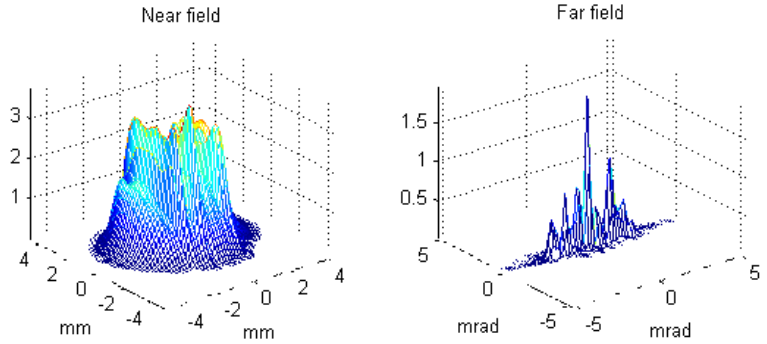

Figure 4.8 Near and far field profiles of the signal from a 1064 nm pumped KTA-based OPO. Notice the large asymmetry in the far field. The beam quality for this beam is M^2~2 and 15 in the x- and y-directions, respectively

4.1.4.1 Seeded OPO

Seeding the OPO with a high quality beam may help improving the OPO beam quality. This effect was simulated for a 1064 nm pumped singly resonant OPO with one 40 mm KTA crystal with double-pass pump, flat mirrors with 50% signal output coupling, and type 2 PM. The 120 mJ pump beam had a pulse length of 6 ns and a FW1/e^2M width of 6 mm. For simplicity, seeding was simulated on the idler wavelength, as the input mirror had 100% transmission on this wavelength. The seed beam had perfect spatial overlap with the pump beam. Figure 4.9 summarizes the OPO signal performance.

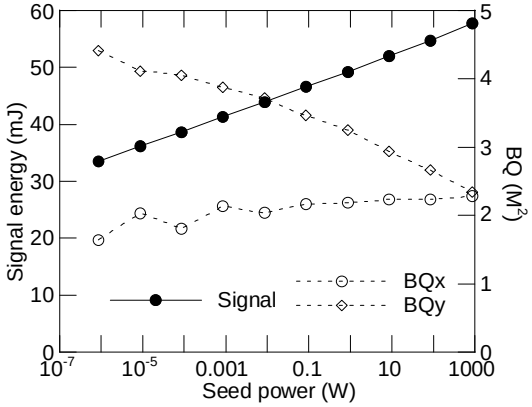

Figure 4.9 Summary of simulated OPO performance as function of CW seed power at the idler wavelength

As expected, seeding improves performance of the OPO, but to obtain a symmetric signal beam, almost 1000 W of seed power at the idler wavelength is necessary. Seeding on the signal wavelength would probably require less intracavity seed power, but for a linear resonator this would have to be transmitted through a highly reflective input mirror in a linear resonator, still

making the required power high. Alternatively, signal wavelength seeding could be injected through the output coupler in a ring geometry, adding complexity and cost to the system. Partly because of this and partly because we consider the concept with two different crystals in the OPO developed in this work to be more promising in terms of OPO performance, we chose not to pursue the seeded OPO-approach further in this work.

4.1.4.2 Elliptic pump beam

By using an elliptic pump beam, the beam size in the non-critical direction can be reduced while the beam area, and hence the pump fluence, is kept constant. This is done by increasing the beam diameter in the other direction so that the product of the diameters is constant. In Figure 4.10, the performance of a KTA-based 532 nm pumped OPO is shown as function of the ratio of the axes of the elliptic cross section of the pump beam, *a/b*. We see that the asymmetry is reduced with increasing ratio, but also that the beam quality in the direction of walk-off is reduced. At a ratio of 10-15, the asymmetry in the beam quality vanishes. However, at this point the beam diameters are approximately 20 mm by 2 mm, and since it is difficult to obtain crystals with >20 mm aperture, we disregard this option to remove astigmatism.[5]

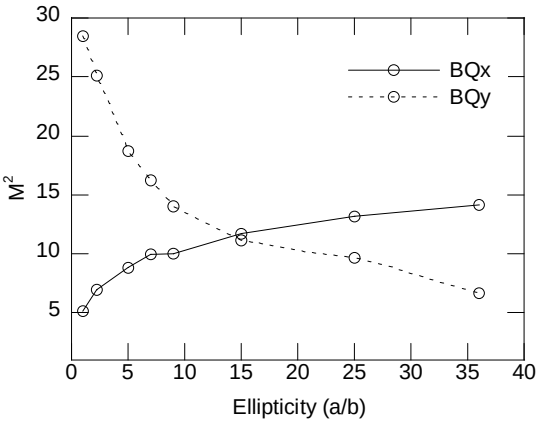

Figure 4.10 Beam quality as function of ratio of the beam diameters of the elliptic pump beam for an OPO with constant beam area. Ratio = 1 corresponds to a circular 6 mm diameter pump beam. The output energy was constant at ~40 mJ in the simulations

4.1.4.3 Unstable resonator

Another approach for the improvement of the beam quality is to configure an unstable resonator, either in the non-critical, or in both directions. Figure 4.11 presents simulation results for a linear KTA OPO with a positive branch confocal unstable resonator [38]. In this resonator, the curved cavity mirrors have a common focal point, and the beam is magnified during one round trip given by the absolute value of the ratio of the radii of curvature of the two mirrors. In Figure 4.11, the performance of a KTA-based OPO with two 25 mm crystals in a walk-off compensating geometry and with 120 mJ pump energy in a 4.4 mm diameter beam is plotted as function of this.

[5] Apertures like this can probably be obtained with periodically poled crystals, but such crystals cannot be used in the experiments presented here because they do not have walk-off and therefore the beam quality in the wide direction will be much poorer than simulated here

The beam quality in the non-critical direction is clearly improved as the magnification (and hence diffraction losses) increases. This resonator geometry requires single-pass pumping as phase matching in the nonlinear crystal is not achieved in the return pass. The single-pass pump geometry leads to relatively low conversion efficiency. Another drawback hampering this approach is the difficulty of alignment.

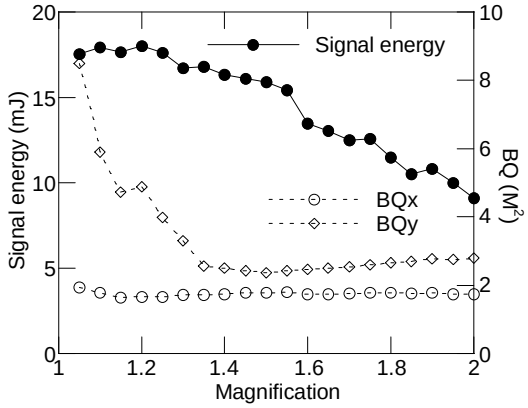

Figure 4.11 Signal pulse energy and, beam quality in the critical (x) and non- critical (y) directions as functions of resonator magnification in a singly resonant walk-off compensated OPO consisting of two 25 mm KTA crystals pumped by 120 mJ at 1064 nm with 4.4 mm pump beam diameter

4.1.4.4 Orthogonal critical planes approach

As discussed in Chapter 3, using two different nonlinear crystals type 2 phase matched for the same interaction, but with orthogonal critical planes can be a simple way of improving the beam quality of an OPO. A possible layout of such an OPO with indication of axis of rotation required for angle tuning for the different crystals is shown in Figure 4.12.

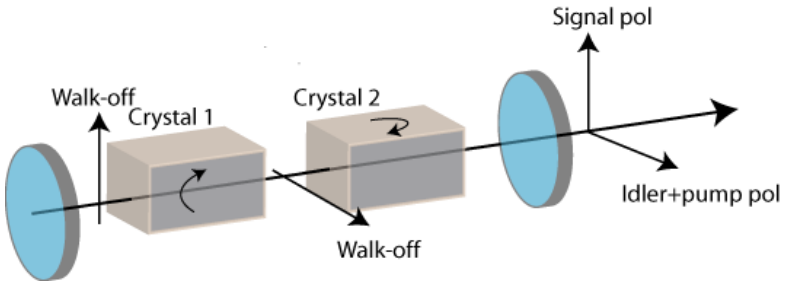

Figure 4.12 Sketch of directions of polarization for critical collinear type 2 PM in the orthogonal critical planes approach

As was explained in Section 3.4.7, such an OPO can be built using KTA (or one of its isomorphs) and BBO. Figure 4.13 shows the performance of a singly resonant OPO consisting of a 30 mm KTA crystal and a BBO crystal of variable length. The 120 mJ pump pulse is double-passed and the beam diameter is 6 mm. The BBO has significant absorption in the infrared. In the simulations, an idler absorption of 190 m^{-1} was used, which is the absorption at the 2.84 µm idler

wavelength corresponding to a 1700 nm signal. Similar behavior as shown in Figure 4.13 was seen in simulations both without idler absorption and with even stronger idler absorption. We note that the inclusion of a BBO crystal in the OPO dramatically improves the beam quality in the non-critical direction in KTA, and that a symmetrical beam is obtained for BBO lengths from 10 mm and above. We also note that increasing the BBO length increases the OPO signal performance in spite of the strong idler absorption (~5 mm absorption length). Figure 4.13 clearly illustrates that the idea of orthogonal critical planes works and it will therefore be employed further in this work.

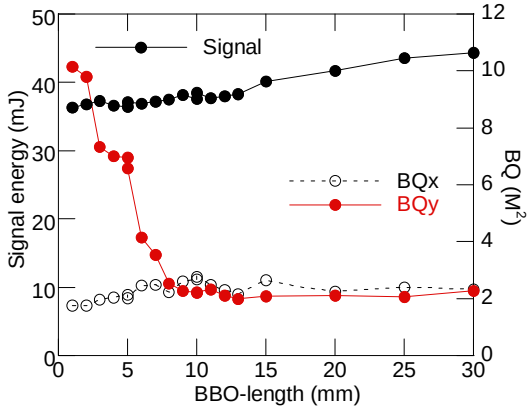

Figure 4.13 Signal beam quality from a singly resonant linear OPO with 30 mm KTA as function of BBO length. The pump beam was 6 mm diameter, and the pump energy was 120 mJ, while the signal output coupling was 50%. The idler absorption was 190 m^{-1} in the BBO crystal

To achieve a symmetric beam quality, the walk-off distance in both directions should be approximately the same. This can be obtained by adjusting the relative lengths between the different crystals according to the intrinsic walk-off properties. In Figure 4.14, the ratio of walk-off angles in KTA and BBO is shown as function of OPO signal wavelength. We note that for the 532 nm pumped OPO, the crystals should be approximately of equal length, while for the 1064 nm pumped OPO, the appropriate BBO length should be approximately 70 % of the KTA length. For the OPO in Figure 4.13, the ideal BBO length should be ~20 mm. However, as Figure 4.13 indicates, the tolerance of the beam quality to the BBO crystal length is relatively large. The ratio can nevertheless be used as a rule of thumb in the design of OPOs based on this technique.

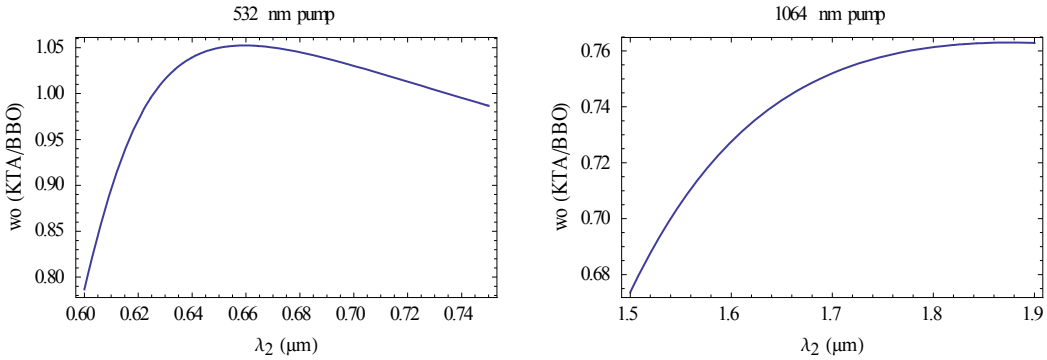

Figure 4.14 Ratio of walk-off angles in KTA and BBO plotted as function of signal wavelength for the two OPOs in consideration in this work

In the following sections we will use these results to optimize the 532 nm and 1064 nm pumped OPOs further.

4.2 1064 nm pumped OPO

Having decided on a linear resonator with double pass pump and with one KTA crystal and one BBO crystal, the other parameters to determine are the pump beam size, the crystal lengths and output coupling. The pump beam size is given by the maximum allowed fluence and the maximum pump energy (but must be calculated for all beams combined). For 120 mJ pump energy, the beam diameter should be on the order of 6 mm, which has also been used so far in the simulations.

In Figure 4.14, we further observed that the BBO to KTA length ratio should be ~0.7. Using this, the final optimization of the OPO can be performed. Typically, the OPO efficiency will increase with increasing crystal length, but longer crystals will also increase back conversion in the more intense parts of the beams, giving a poorer beam quality. Figure 4.15 shows the OPO performance as function of KTA length for 50% output coupling with 120 mJ pumping in a 6 mm diameter beam. As expected, longer crystals give more output energy. Taking the decrease in beam quality at longer crystal lengths, and also that the crystal cost is more or less proportional to the crystal volume, a good choice of KTA length appears to be 30-40 mm. The corresponding BBO length in the simulations is 21-28 mm.

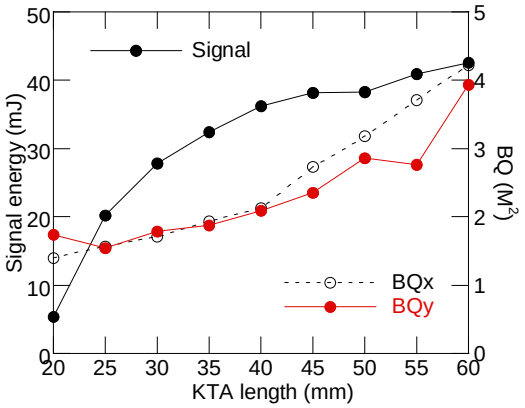

Figure 4.15 Signal energy and beam quality as function of crystal length for 120 mJ pump energy in a 6 mm diameter beam. The BBO length is fixed to 70 % of the variable KTA crystal length in a singly resonant OPO with 50% output coupling.

Simulated OPO performance as function of signal reflectivity at the output mirror is shown in Figure 4.16 for two different KTA lengths. For the 40 mm KTA/ 28 mm BBO OPO, the output energy is not very sensitive to the output coupling. However, the intracavity fluence (not shown) depends strongly on the output coupling, and is, for example ~50% higher for R = 70% than for R = 50%. Based on this and the results in Figure 4.16, it seems that R = 30% at the signal is a good choice for this OPO. If the crystals are shorter, the OPO operates closer to threshold and is more sensitive to the output coupling. For an OPO with 30 mm KTA and 21 mm BBO, R = 50% is recommended.

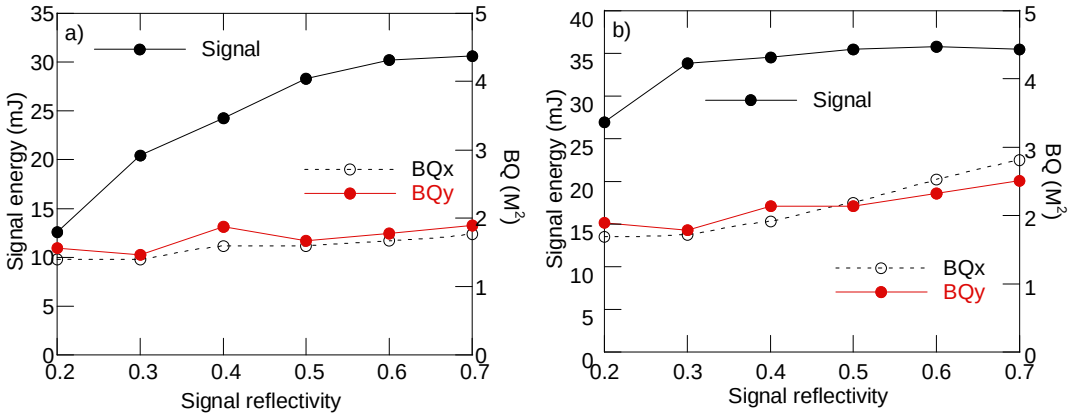

Figure 4.16 Simulated KTA-BBO OPO performance as function of signal output coupling with 120 mJ pump energy in a 6 mm diameter beam with double-pass pumping. a) 30 mm KTA / 21 mm BBO. b) 40 mm KTA / 28 mm BBO.

4.2.1 Tuning and idler absorption

BBO has poor transmission at wavelengths above 2.5 µm, as is shown in Figure 4.17a. Figure 4.17b shows the BBO idler absorption as function of OPO signal wavelength. Also shown is the corresponding UV wavelength after SFG with 355 nm. At 1.8 µm signal wavelength, the idler absorption is ~120 m^{-1} and at 1.6 µm signal wavelength, the idler absorption is ~500 m^{-1}.

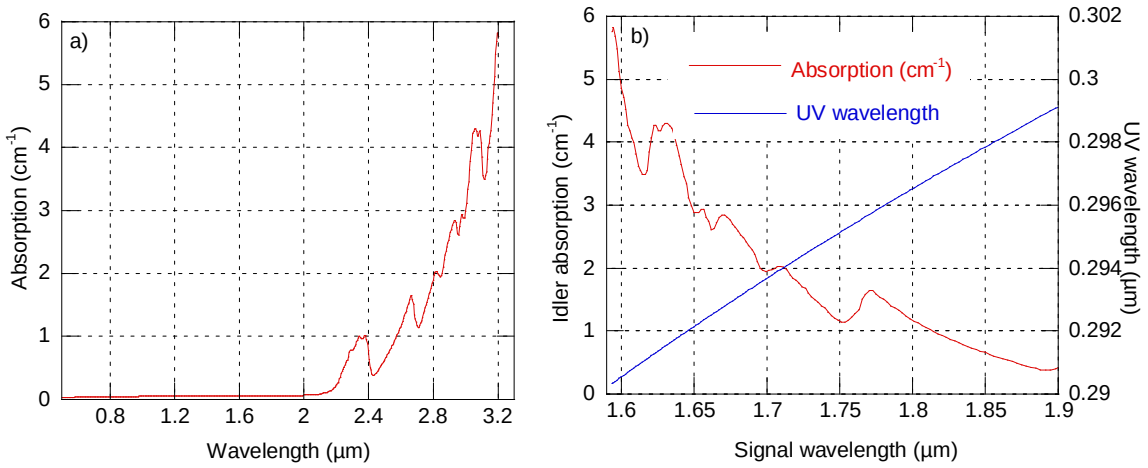

Figure 4.17 a) Absorption in BBO as function of wavelength. b) Idler absorption as function of signal wavelength for 1064 nm pump. Also plotted is the resulting UV wavelength when the signal is summed with 355 nm in a SFG stage

Idler absorption does not need to result in a reduced performance. We have previously seen that the signal performance can be improved with increasing idler absorption for low pulse rate OPOs because longer crystals can be chosen before back conversion becomes a problem [6]. Below, we have simulated the KTA-BBO OPO with varying idler absorption. Both the 30 mm KTA/21 mm BBO with 50% signal reflectivity and the 40 mm KTA/28 mm BBO with 30% signal reflectivity are simulated. The idler absorption was varied from 0 to 450 m^{-1} while all other parameters were fixed. Figure 4.18 summarizes the results. As expected, we see that the beam quality improves as the idler absorption increases from zero. The signal energy decreases indicating that the crystal length and output coupling is well chosen for an OPO with fairly low idler losses. We notice, however, that the beam asymmetry increases as the idler absorption increases above ~200 m^{-1}. In type 2 PM, the signal and idler have walk-off with respect to each other. This helps increase the spatial coherence and thus the beam quality. When idler absorption increases, the length in which this spatial coherence can be increased is reduced, and hence the beam quality is reduced.

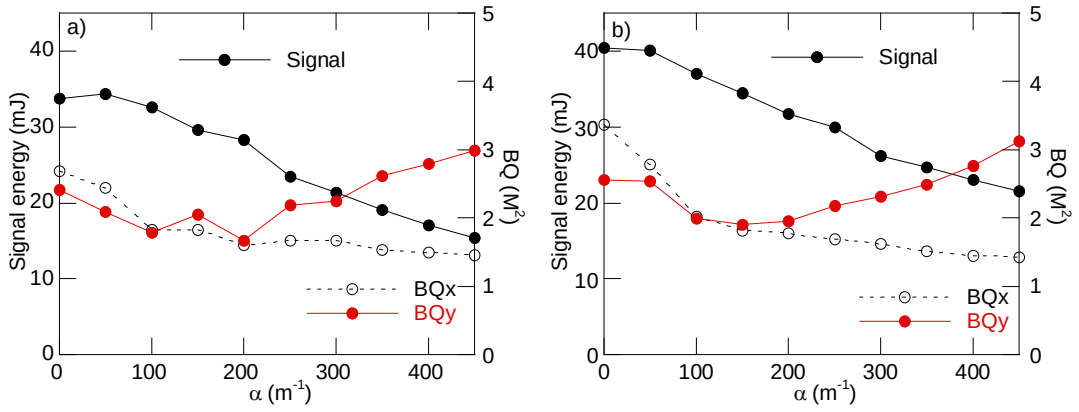

Figure 4.18 OPO signal performance as function of idler absorption in BBO. a) 30 mm KTA / 21 mm BBO with 50% signal reflectivity. b) 40 mm KTA / 28 mm BBO with 30% signal reflectivity

The beam asymmetry can be improved even for very high absorption levels. As strong idler absorption reduces the beam quality improvement in BBO, a longer BBO crystals is then required. This is shown in Figure 4.19a, where a 40 mm KTA OPO with variable BBO length is simulated for 400 m^{-1} idler absorption in BBO. While the beam quality is improved, the output energy drops significantly when increasing the BBO length to 50 mm. This can to some extent be compensated for by using a longer KTA crystal, and Figure 4.19b shows results from similar simulations with 50 mm KTA. However, this requires even longer BBO crystals, still limiting the signal output energy. Consequently, it appears that if a symmetrical beam quality is required for very high idler absorption levels, this will come at the expense of conversion efficiency. For the OPO in question in this work, the ~200 m^{-1} idler absorption when operating around 1700 nm signal wavelength seems to work well.

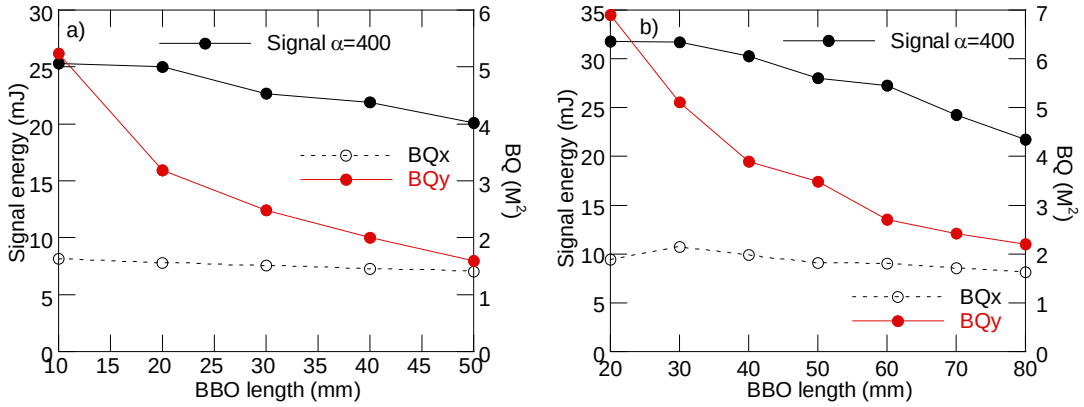

Figure 4.19 OPO signal performance for 400 m^{-1} idler absorption in BBO for 40 mm KTA and 30% signal reflectivity as function of BBO length

4.2.2 Pump bandwidth

The OPO performance depends on the pump bandwidth. In Figure 4.20a, the OPO performance at 120 mJ pump energy is shown as function of pump bandwidth for the 40 mm KTA/28 mm BBO OPO. It appears that up to 50 GHz bandwidth can be tolerated without loss in OPO performance.[6] Interestingly, not only the signal energy, but also the beam quality becomes poorer for higher pump bandwidth. This only applies to the beam quality in the direction where the far field divergence is limited by the BBO acceptance angle. We believe that this stems from temporal walk-off between the pump and the signal/idler in BBO. If the group index of the pump is significantly different from that of the signal or idler, the phase of the broad-band pump beam will become uncorrelated with the signal after some distance through BBO. This will reduce the spatial filtering effect that is a result of spatial walk-off in BBO. If the pump bandwidth increases, this correlation distance and hence beam quality, decreases.

Figure 4.21 shows the group indices as function of signal wavelength for KTA and BBO for this OPO. At 1700 nm signal wavelength, the group indices of the pump, signal and idler are 1.64, 1.67 and 1.68, respectively. If the OPO is tuned to 1800 nm signal wavelength, the corresponding

[6] The bandwidth of the laser that is available for the experiments is about 20 GHz.

group indices are 1.64, 1.67 and 1.66 (pump, signal, and idler). Hence the difference in group index and thereby the temporal walk-off are reduced. Figure 4.20b shows corresponding simulations for this OPO. The idler absorption is lower, and the overall beam quality decrease slightly at low pump bandwidth. We note, however, that the beam asymmetry at higher pump bandwidths is dramatically smaller than for 1700 nm signal.

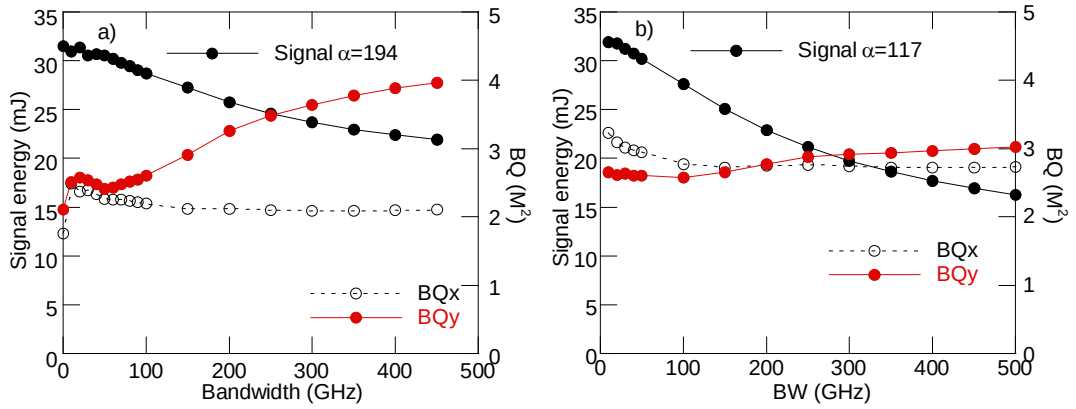

Figure 4.20 OPO signal energy and beam quality as function of pump bandwidth for 1700 nm signal (a) and 1800 nm signal (b). The beam quality is limited by the KTA crystal in the x-direction and the BBO-crystal in the y-direction

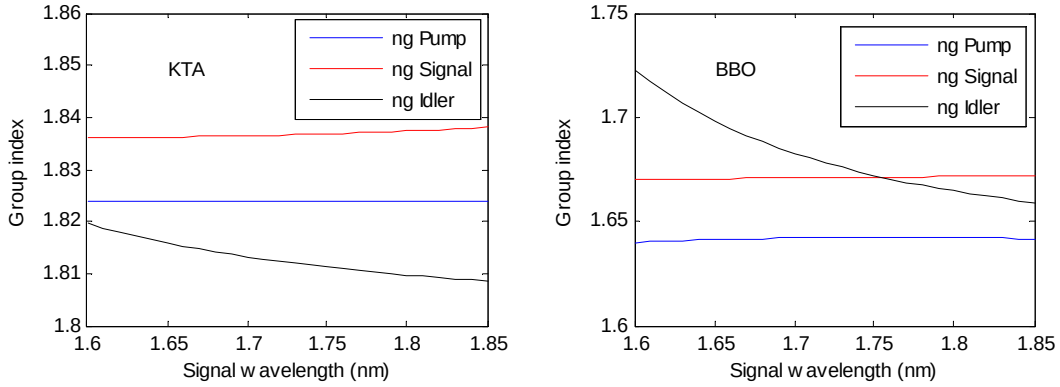

Figure 4.21 Calculated group indices of KTA [39] and BBO [40] as function of signal wavelength for a type 2 phase matched 1064 nm pumped OPO

Figure 4.22 shows the OPO signal spectrum for 10, 50 and 300 GHz pump bandwidth. We note that the signal spectrum varies only little with pump bandwidth, and the 100-150 GHz signal bandwidth is below the acceptance bandwidth of the SFG process to be studied in Chapter 5 (~230 GHz for a 5 mm long BBO crystal).

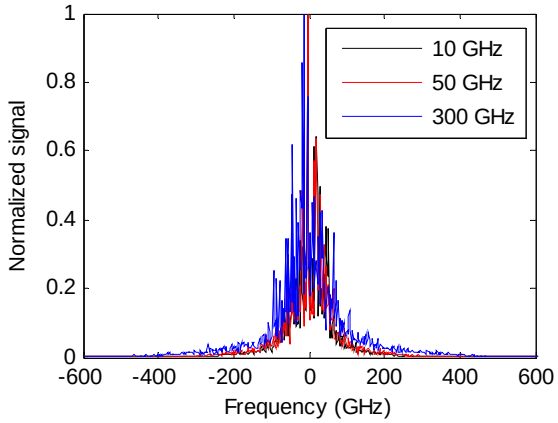

Figure 4.22 OPO signal spectrum for three different pump bandwidths for 1700 nm signal

4.2.3 Summary of 1064 nm OPO design

The design recommendations for the 1064 nm pumped OPO can be summarized as:

- Linear resonator with flat mirrors, rotated critical planes, double pass pump OPO
- Smallest possible air gaps to reduce signal build-up time
- 30-40 mm KTA crystal length
- 20-28 mm (accordingly) BBO crystal length
- 30-50 % output mirror signal reflectivity (higher for shorter crystals)
- OPO design valid for ~ 1700 nm signal wavelength. Operation at shorter wavelengths is possible, but may lead to reduced output energy and beam quality.

With this design, about 30 mJ of 1700 nm signal with good beam quality (M^2 ~2) can be expected from a KTA-BBO based OPO pumped by a pump beam with <50 GHz bandwidth. Operation at shorter wavelengths is possible, but at the expense of signal energy and beam quality.

4.3 1064 nm pumped MOPA

The alternative approach from the high energy OPO is to apply a MOPA architecture. Although this is much more complicated than the OPO approach described above, it may be necessary if wavelengths close to or below 290 nm after the SFG stage are required, as this approach does not need to use IR absorbing BBO crystals. As we recommended to use an OPO described previously in this chapter in the experiments, this section is brief. We have simulated a type 2 phase matched KTA-based OPO-OPA system with emphasis on beam quality and conversion efficiency assuming that 120 mJ of pump energy is available at 1064 nm (the rest of the 1064 nm energy is used to generate 355 nm).

In Figure 4.23, the performance of an OPO consisting of two 15 mm long KTA crystals oriented for walk-off compensation, is shown as function of pump beam size when the peak pump fluence is kept constant at 0.8 J/cm^2. The pump was double-passed through the crystals and the output reflectivity of the singly resonant OPO was 70%, giving a total peak fluence around 2-2.5 J/cm^2 in all simulations. We note that even for small pump beam sizes, an asymmetry in beam quality

can be observed. The transversal walk-off distance through the 15 mm crystal is 0.6 mm, making the effective overlap region between signal and pump small at the smallest beam diameters. We choose to use 0.6 mm diameter as the starting point for the OPA simulations.

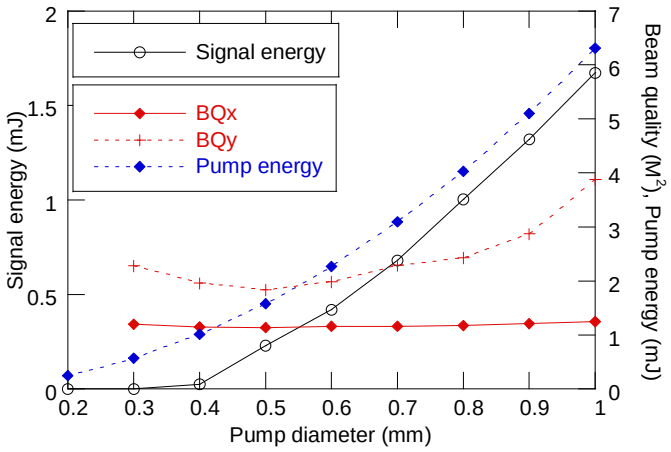

Figure 4.23 Simulated performance of a type 2 phase matched KTA OPO as function of pump diameter for 0.8 J/cm^2 pump fluence

The ~0.4 mJ signal input from the seed OPO simulations was magnified to overlap with the 3 mm diameter 120 mJ OPA pump beam. The peak pump fluence in the OPA simulations was 1.7 J/cm^2 (this can be higher than in the OPO because there is no resonator or double-passing of the pump). As the peak of the OPO pulse is ~3 ns behind the peak of the pump pulse (see Figure 4.24a), the pump pulse needs to be delayed with respect to the signal pulse to have optimal temporal overlap in the OPA simulations. The effect of pump pulse delay was simulated with an OPA consisting of four 20 mm long KTA crystals oriented in an alternating walk-off compensating pattern, as is discussed later in this section. The optimal delay in this case was found to be 4 ns, as is shown in Figure 4.24b. We notice that there is little change in performance of the OPA over ±1 ns variation in the delay off this optimal point. The difference in optimal delay (4 ns) and distance between peak power (~3 ns) is probably due to the long tail of the seed pulse caused by the relatively high Q seed OPO resonator.

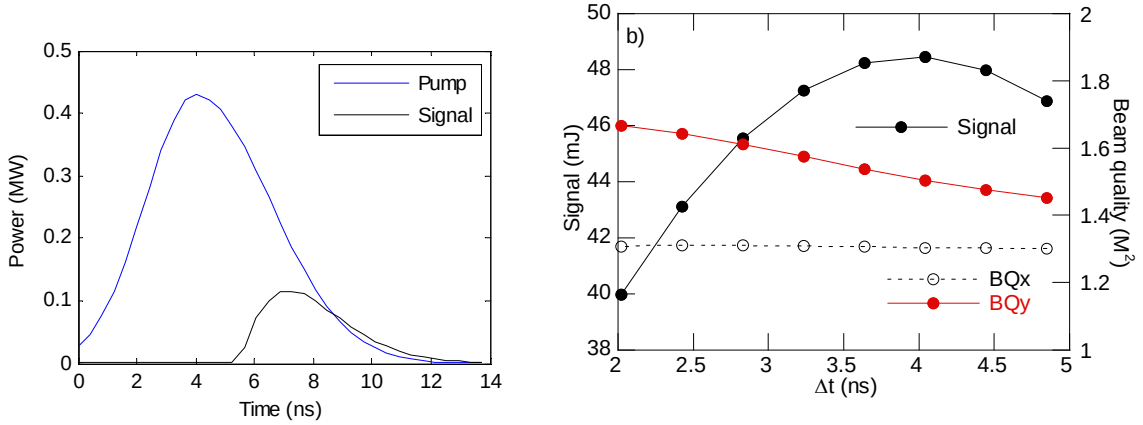

Figure 4.24 Temporal evolution of pump and signal pulse in the seed OPO (left). OPA performance as function of pump delay with respect to signal pulse (right)

To have sufficient gain in the OPA, the total crystal length needs to be rather long. Total KTA lengths may be as high as 80-100 mm. As the walk-off distance between signal and pump is ~1 mm through 25 mm KTA, it is necessary to use several crystals with walk-off compensation to obtain the necessary interaction length. Further, it is well known that back conversion may reduce the performance of an OPA [12]. Back conversion can be reduced by removing the idler between the crystals. This can be accomplished by use of dichroic mirrors [12]. In Figure 4.25, the performance of a KTA based OPA with two crystals in a walk-off compensating geometry is shown as function of total KTA length with and without idler removal between the KTA crystals. It is clear that for short crystals, the idler beam is necessary to have sufficient amplification, but for longer crystals, removing idler reduces back conversion and hence improves the performance of the OPA.

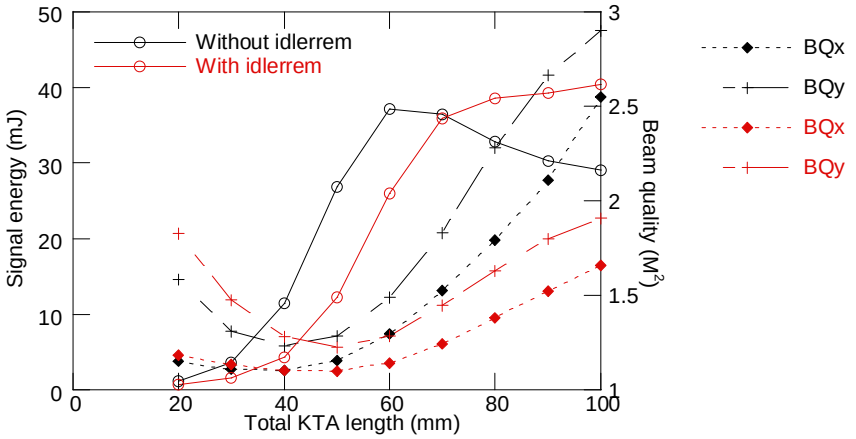

Figure 4.25 Simulated OPA performance as function of total KTA length for an OPA with two KTA crystals in walk-off compensating geometry with (red curves) and without (black curves) idler removal between the crystals

As the optimal total KTA length is well above 50 mm, more than two KTA crystals may be necessary to have sufficient spatial overlap between the pump and the signal. In Figure 4.26, the performance of OPAs with 2, 3 and 4 KTA crystals are compared as function of total KTA length. The idler was removed before the last crystal in all configurations. We notice that the OPAs perform similarly for low crystal lengths, and that more crystals are better for longer total crystal lengths. The performance of the 2 crystal OPA becomes poorer than the rest for >60 mm total crystal length, while the 3 and 4 crystal OPAs performs similarly throughout the simulated length range.

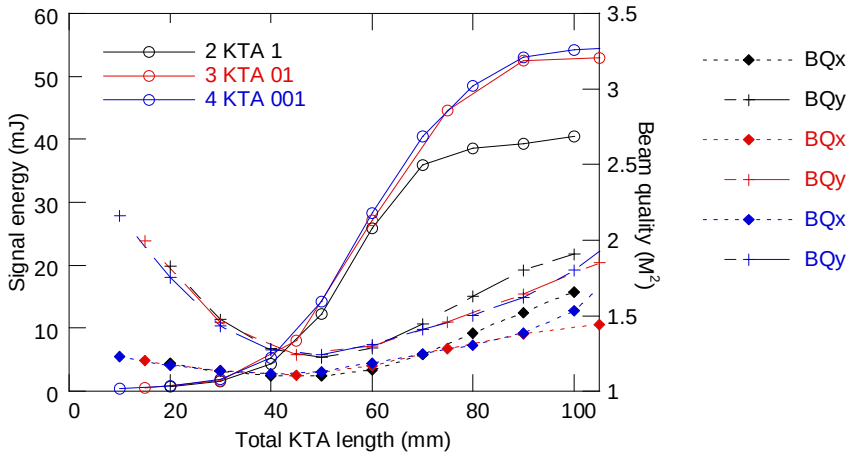

Figure 4.26 Comparison of performance of OPAs with 2, 3 and 4 KTA crystals as function of total KTA length. Idler beam was removed before the last crystal in all configurations

As we have previously seen that idler removal at more than one point may be advantageous in an OPA [12], the 4 crystal KTA OPA was simulated with idler removal between one or more of the KTA crystals. Figure 4.27 compares the performance of these 4 crystal OPAs. We note that removing the idler at more positions leads to a requirement for longer crystals, but also that the OPA performs better with longer crystals. We do, however, note that the improvement in performance with more idler output coupling is marginal, and can likely not justify the increased crystal cost and complexity. Therefore we recommend only using idler removal before the last crystal in the OPA.

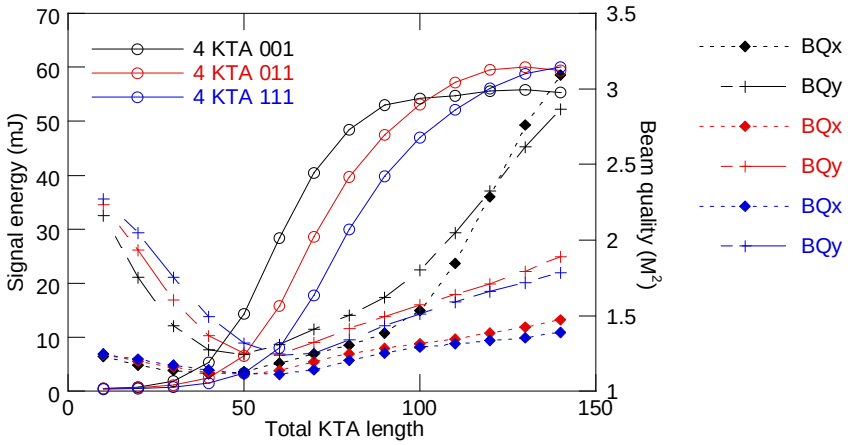

Figure 4.27 Comparison of performance of 4-crystal OPAs with idler removal at one or more positions. The three numbers after KTA in the legend indicate the three crystal interfaces in the OPA. 0 means no idler removal and 1 means idler removal, e.g. 001 means removal of idler only before the last crystal

Based on the simulations in this section, the following MOPA design is recommended:

- OPO
  - Crystals: 2 x 15 mm KTA cut for type 2 PM
  - Double-pass pump, singly resonant operation, 70% reflectivity on signal
  - 0.6 mm diameter pump, 2.4 mJ pump energy (near field of laser)
- OPA
  - Delay: OPA pump delayed 4 ± 1 ns (120 ± 30 cm) relative to OPO pump
  - Crystals: 4 x 20 mm KTA crystals cut for type 2 PM
  - 3 mm pump beam diameter, 117 mJ pump
  - Signal beam size from OPO magnified 5x
  - Idler removal before last KTA crystal

A MOPA designed according to these criteria should be able to generate ~50 mJ of 1600 nm signal with high beam quality, $M^2 < 2$ in both directions.

4.4 532 nm pumped OPO

As was seen in Figure 4.14, the walk-off angle is approximately equal in KTA and BBO when tuned to type 2 PM for a 532 nm pumped OPO. As a starting point we therefore choose to use equal KTA and BBO crystal lengths in the simulations. Figure 4.28 shows the performance of a singly resonant with 40% output reflectivity, double-pass pump KTA-BBO OPO tuned to 670 nm as function of crystal length. At this wavelength, the idler absorption in BBO is ~100 m^{-1}. The pump beam diameter is still 6 mm, making the peak fluence in the OPO ~2 J/cm^2. We note that longer crystals lead to more output energy, but also a poorer beam quality. 20 mm crystal length therefore seems like a good choice for this OPO.

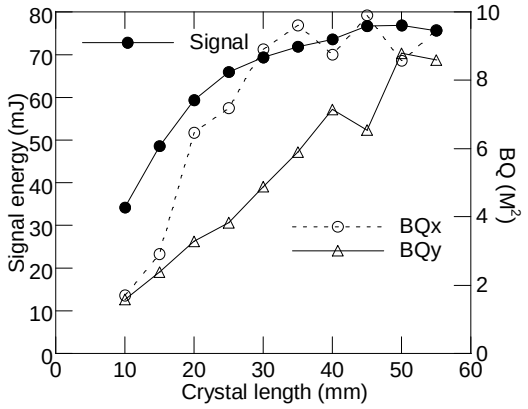

Figure 4.28 Simulated performance of a KTA-BBO OPO as function of KTA and BBO crystal length for 40% reflectivity at the signal wavelength. The other details of the simulations are given in the text

Figure 4.29 shows the simulated performance of the KTA-BBO OPO for fixed 20 mm KTA length and 40% signal reflectivity, as function of BBO length. Although the improvement in beam quality appears for relatively short crystals, we note that increased BBO length also contributes to the signal energy without loss in beam quality. Therefore, it seems like a good choice to use similar lengths for the KTA and BBO crystals.

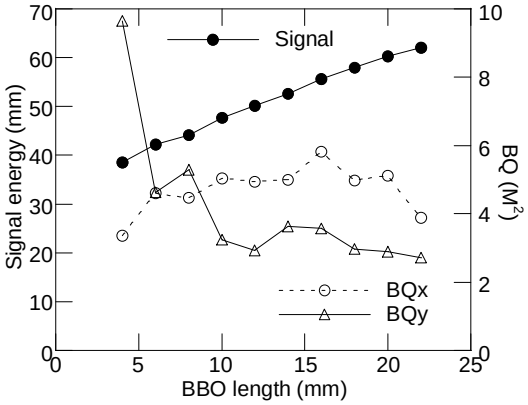

Figure 4.29 Simulated performance of a KTA-BBO OPO with 20 mm KTA length and 40% signal reflectivity as function of BBO crystal length. The other details of the simulations are given in the text

Figure 4.30 shows the KTA-BBO OPO performance for 20 mm KTA and BBO crystal lengths as function of output reflectivity. It appears that both the intracavity fluence and the beam quality becomes significantly worse for reflectivities 40-50% and higher. Based on this, 30% signal reflectivity is recommended.

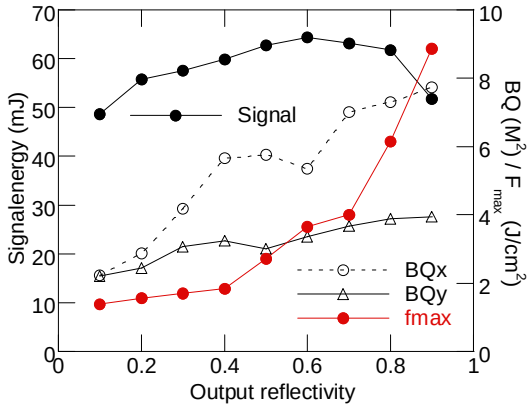

Figure 4.30 Simulated performance of a KTA-BBO OPO with 20 mm KTA and 20 mm BBO as function of output reflectivity at the signal wavelength. The other details of the simulations are given in the text

4.4.1 Tuning

Since the OPO idler wavelength is the only energy that is 'intrinsically lost' in both UV-schemes presented in this work, the OPO idler wavelengths will be the same for both the 1064 nm pumped OPO and the 532 nm pumped OPO for the same final UV wavelength. Thus, the absorption losses on the idler wavelength will also be the same. Figure 4.31a shows the BBO idler absorption as function of signal wavelength. The corresponding UV wavelength after the SFG stage is also indicated. Figure 4.31b shows the simulated performance for a 120 mJ 532 nm pumped OPO with 20 mm long KTA and BBO crystals and 30% signal reflectivity on the output coupler as function of idler absorption. We see that for this OPO, some idler absorption leads to improved performance. This is not unexpected, and is in agreement with previous results [6]. If BBO had had no idler absorption, the optimal crystal lengths for the OPO had been shorter. The results in Figure 4.31 indicate that it should be possible to tune the OPO to rather short wavelengths still maintaining a reasonably high efficiency. It should be noted that the results in Figure 4.31b are valid for single shot or low pulse rate. The 10 Hz pulse rate of the pump laser to be used in later work is probably within the valid range of the simulations.

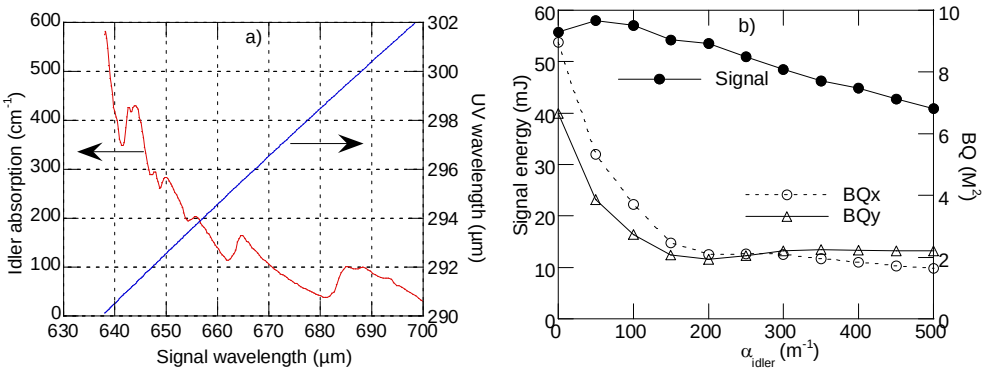

Figure 4.31 a) Idler absorption in BBO as function of signal wavelength. Also indicated is the resulting UV wavelength after SFG with 532 nm. b) Simulated KTA-BBO OPO performance as function of idler absorption for 20 mm crystal lengths and 30% signal reflectivity

4.4.2 Pump bandwidth

The effect of an amplitude modulated pump was simulated for the 20 mm KTA/20 mm BBO OPO with 30% signal reflectivity at the output coupler. Figure 4.32 shows that the signal output energy decreases about 20% when the pump bandwidth is increased from SLM to 100 GHz ($FWe^{-2}M$), while the beam quality was unaffected for bandwidths up to ~50 GHz above which the beam quality in the critical direction of KTA deteriorates. As was discussed in Section 4.2.2, this can be explained by temporal walk-off between the pump and the signal/idler. Figure 4.33 shows the group indices of KTA and BBO for this OPO as function of signal wavelength. We note that while the difference between pump and signal is small in BBO, there is a relatively large difference in KTA. This can explain why it is the beam quality in the critical direction in KTA, and not in BBO, that is affected by the higher pump bandwidth in this OPO. Also shown in Figure 4.32 is the normalized signal spectrum. We note that this spectrum is more affected by the pump bandwidth than was the case for the 1064 nm pumped OPO in Figure 4.22. However, the signal bandwidth for 50 GHz pump bandwidth is ~100 GHz which is well below the acceptance bandwidth for the SFG process to be discussed in Chapter 5 (~280 GHz at 670 nm for a 5mm long BBO crystal).

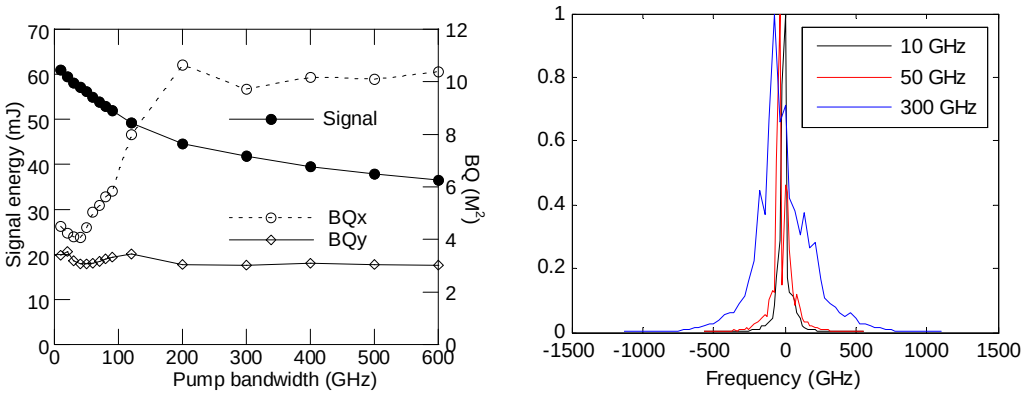

Figure 4.32 Left: Calculated performance of a 532 nm pumped OPO as function of pump bandwidth ($FWe^{-2}M$). Right: Normalized signal spectra at 670 nm for three different pump bandwidth

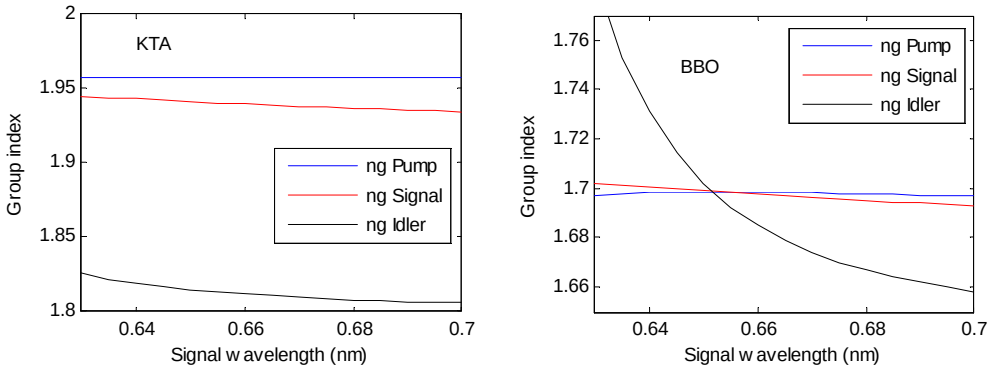

Figure 4.33 Calculated group indices in KTA [40] and BBO [40] as function of signal wavelength for a 532 nm pumped type 2 phase matched OPO

4.4.3 Summary of 532 nm OPO design

The design recommendations for the 532 nm pumped OPO can be summarized as:

- Linear resonator with flat mirrors, rotated critical planes, double pass pump OPO
- Smallest possible air gaps to reduce signal build-up time
- 20 mm KTA and BBO crystal lengths
- 30 % output mirror signal reflectivity
- OPO design valid for ~ 670 nm signal wavelength. Operation at shorter wavelengths is possible, but may lead to reduced output energy. Longer crystals may be necessary in this case.

With these parameters, 55-60 mJ of 670 nm light with good beam quality ($M^2 < 3$) could be expected using 120 mJ pump light and <20 GHz bandwidth at 532 nm.

4.5 532 nm pumped MOPA

In this section a KTA-based MOPA system for conversion of 532 nm to 640-670 nm is studied. It is assumed that a total of 120 mJ energy at 532 nm in a 5 ns pulse and an order 6 super-Gaussian beam is used to pump the MOPA stage.

4.5.1 Master Oscillator

The gain in KTA is sufficient for the 532 nm pumped OPO to be operated with single-pass pump. Hence, the incident pump intensity can be increased still keeping the total peak fluence below damage threshold. In the simulations, the incident peak pump fluence has been set to 1.2 J/cm^2. Figure 4.34 shows the simulated performance of a small beam single-pass pumped KTA OPO as function of KTA crystal length for two different pump diameters. The OPO consists of two equal KTA crystals oriented in a walk-off compensating geometry. The crystal length in Figure 4.34 is the length of one KTA crystal; hence the total crystal length is twice this. We note that for the small beam diameter (0.4 mm FWe^{-2}M), the optimal crystal length is around 10 mm, while for the larger diameter (0.8 mm) the beam quality becomes too poor to find an optimal length.

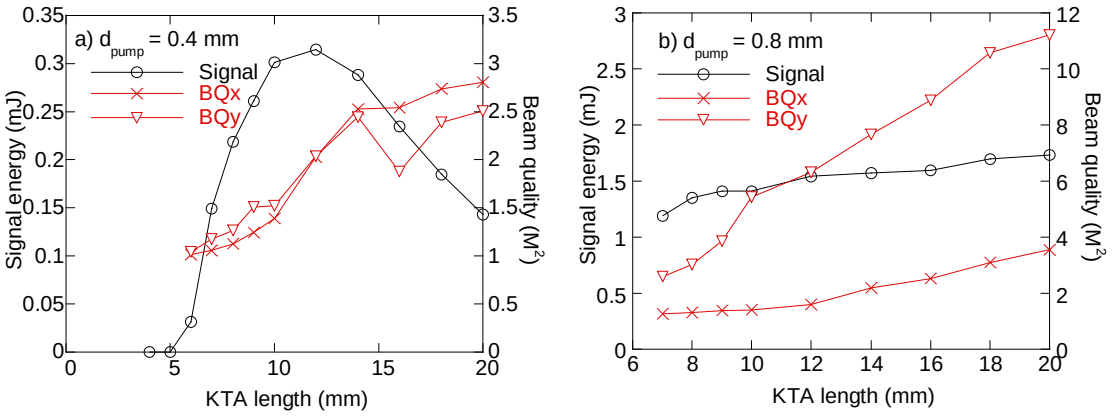

Figure 4.34 Simulated performance of a single-pass pumped singly resonant OPO consisting of two KTA crystals in a walk-off compensating geometry and with 60% output coupling of the signal beam. The OPO is oscillating at 670 nm and is pumped at 532 nm with an order 6 super-Gaussian beam with 1.2 J/cm^2 peak pump fluence. a) With 0.4 mm pump diameter and 1.1 mJ pump energy, 10 mm KTA length combines good beam quality and high conversion efficiency. b) With 0.8 mm pump diameter and 4.3 mJ pump energy, the beam quality is too poor to find an optimal KTA length

Figure 4.35a shows OPO performance as function of pump diameter for two 10 mm KTA crystals and 60% signal output coupling (i.e. 40% reflectivity). We see that when increasing the diameter above 0.4 mm length, a strong asymmetry is growing in the signal beam quality. Figure 4.35b shows OPO performance as function of signal reflectivity at the output coupler. As the reflectivity increases, both the intracavity fluence and the beam asymmetry increase. Hence, a 40% reflectivity (60% output coupling) seems optimal in this case.

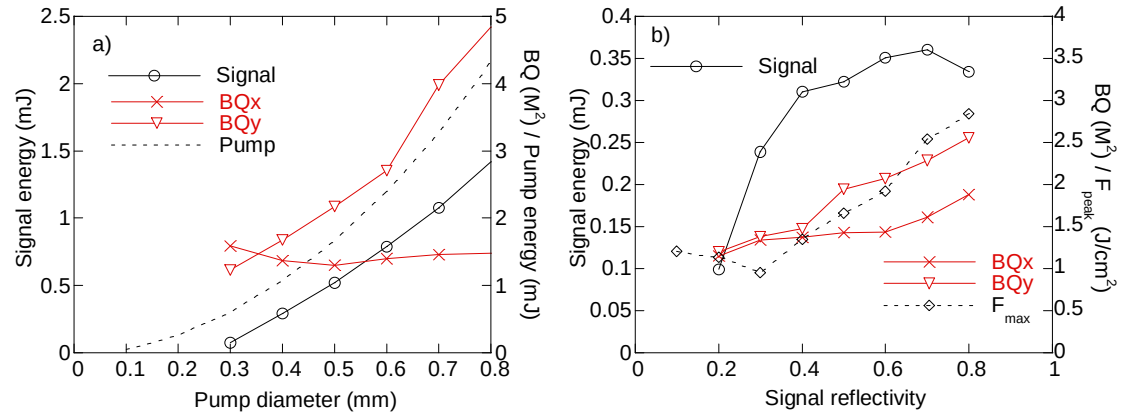

Figure 4.35 Simulated performance of a 532 nm single-pass pumped OPO with two 10 mm KTA crystals in walk-off compensating geometry. a) As a function of pump beam diameter (1.2 J/cm^{2}peak fluence) with 40% output reflectivity of the signal. b) As a function of signal reflectivity at the output coupler for 0.4 mm pump beam diameter (1.1 mJ pump energy)

In the simulations of the amplification stage, we therefore choose a master oscillator consisting of two 10 mm KTA crystals single-pass pumped with 1.1 mJ in a 0.4 mm diameter beam. The OPO is singly resonant with 40% reflectivity on the signal beam.

4.5.2 Power Amplifier

A KTA based optical parametric amplifier is simulated in this section. We assume that 115 mJ of energy is available in a 4 mm diameter ($FWe^{-2}M$) pump beam. The resulting peak pump fluence is 1.3 J/cm^2. Parameters that can be varied is total crystal length, number of crystals with or without walk-off compensation and idler output coupling, as well as the size and delay of the seed beam relative to the pump beam.

In the initial simulations, the 0.3 mJ seed beam is magnified 14 times to match the 4 mm diameter beam size of the pump beam, and the pump beam is delayed 2.1 ns with respect to the seed beam to have overlapping peaks. These parameters are varied later in this section. Figure 4.36 shows the performance of the OPA as function of KTA length for a single KTA crystal. For this geometry, the optimal length is 25-30 mm.

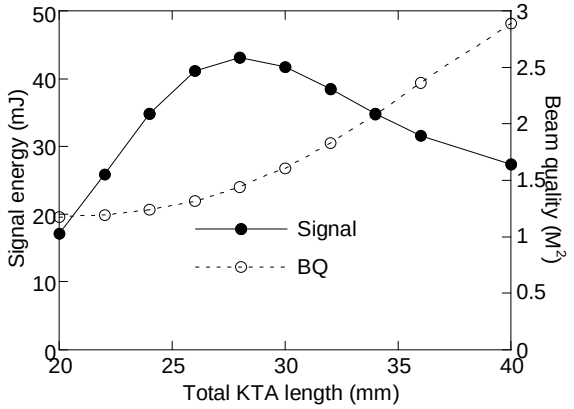

Figure 4.36 Simulated performance of a one-crystal KTA as function of KTA length using the pump beam described in the text and the seed beam from the previous section

Both spatial walk-off between the interacting beams and back-conversion may reduce the performance of the OPA. This can to some extent be mitigated by using more than one crystal in a walk-off compensating geometry and by removing the idler beam between the crystals. In Figure 4.37a, the performance of the single crystal OPA is compared to a two crystal OPA with walk-off compensation as function of total KTA length. It seems clear that walk-off is not important for this combination of crystal length and beam diameters. Also shown is the two-crystal OPA with idler removal between the crystals. This OPA requires somewhat longer crystals, but the performance at the optimal point of operation is not significantly improved. This is probably because back-conversion is most important at the far end of the KTA crystals. An easy way of studying this is to use more and shorter KTA crystals. Figure 4.37b shows simulations of a four-crystal KTA OPA with idler output coupling either after crystal 3 or after both crystals 2 and 3. Again, the required total KTA length increases, but the performance is also

significantly increased. With four 15 mm KTA crystals with idler output coupling after crystals 2 and 3, more than 65 mJ of signal energy can be obtained with good beam quality (M^2~1.7).

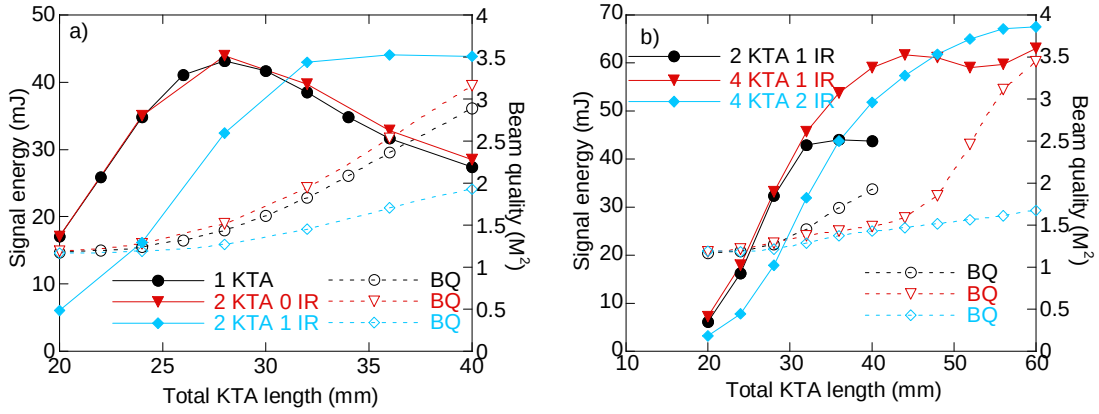

Figure 4.37 Performance of OPAs with different number of crystals and idler output coupling as function of total KTA length. a) Comparison of a one-crystal OPA (1 KTA) with a two-crystal OPA without (2 KTA 0 IR) and with (2 KTA 1 IR) idler output coupling between the crystals. b) Comparison of the two-crystal OPA shown in a) with four-crystal OPAs with idler output coupling after crystal 3 (4 KTA 1 IR) or after both crystals 2 and 3 (4 KTA 2 IR)

The simulations so far have used the optimal beam fitting between the pump and seed beams. It is of interest to see how sensitive the OPA performance is to variations in these fittings. Figure 4.38a shows the temporal curves of the pump and the seed beam coming from the master oscillator. The peak of the seed pulse is approximately 2 ns delayed with respect of the pump pulse. To have optimal overlap in the OPA, the pump pulse then needs to be delayed. Figure 4.38b shows how the performance of the OPA is affected by the pump delay for an OPA with two 16 mm KTA crystals with idler output. We see that one should aim for an approximate temporal overlap, but that a precise adjustment of this parameter is not necessary.

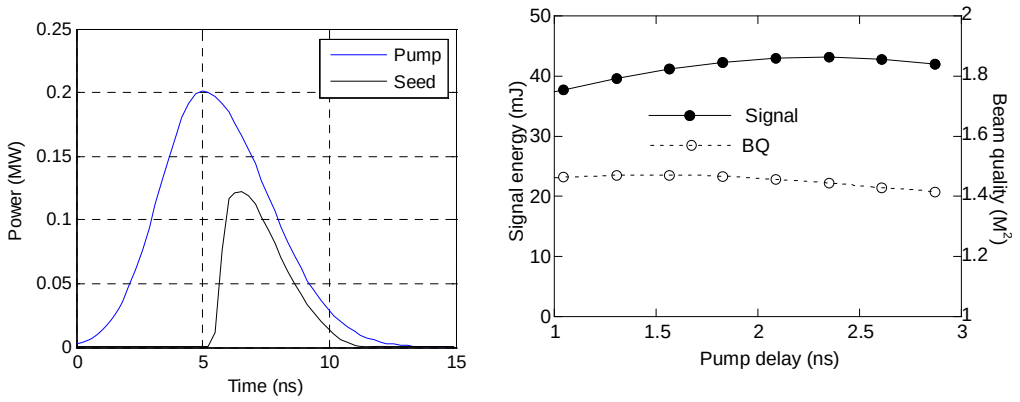

Figure 4.38 a) Plot of the temporal evolution of the pump and the seed pulse from the master oscillator. b) OPA performance as function of pump delay for a 2 x 16 mm KTA OPA with idler output coupling

Figure 4.38b shows that the amplification stage is not very sensitive to the fine adjustment of the relative timing of the seed and pump pulses. This also applies to the size and spatial overlap. Figure 4.39a shows the performance of the 2 x 16 mm KTA OPA with idler output coupling as function of seed position relative to the pump. The performance of the OPA is best when the beams overlap within +/- 1 mm. The size of the pump beam in the OPA is ten times as wide as that in the seed OPO. Figure 4.39b shows that the seed beam should be magnified a factor 10-20, where over-filling the OPA leads to an improved beam quality.

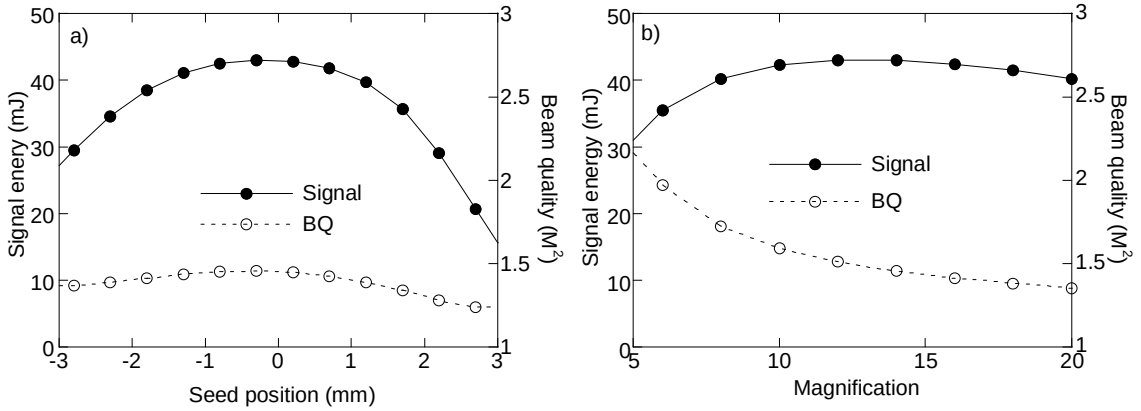

Figure 4.39 a) OPA performance as function of position of the seed beam relative to the pump beam. b) OPA performance as function of seed beam magnification. The OPA is in both cases a 2 x 16 mm KTA OPA with idler output coupling

The OPA is also rather insensitive to the energy of the seed beam. In the simulations above, the energy was ~0.3 mJ. Varying this energy while keeping all other parameters constant gave only a slight increase in output energy for a 4 x 15 mm OPA, from 66 mJ at 0.1 mJ seed to 69 mJ at 0.5 mJ seed. The beam quality remained constant.

4.5.3 Summary

In summary, about 60 mJ at 650 nm with M^2~1.7 can be obtained with 120 mJ of 532 nm pump energy in a MOPA geometry:

Oscillator:

- 2 x 15 mm KTA in walk-off compensating geometry
- 1.1 mJ single-pass pump with 0.4 mm beam diameter
- Singly resonant with R=40% signal output coupling

Amplifier:

- 15 x magnification of seed beam
- 2 ns delay of pump pulse
- 4 x 15 mm KTA crystals in alternate walk-off compensating geometry
- Idler output coupling (removal) after crystal 2 and 3
- 115 mJ pump energy in 4 mm diameter beam

5 Sum frequency generation

This chapter summarizes simulations to optimize the SFG stage following the OPO stage. The SFG stage is pumped by either 355 nm or 532 nm combined with the signal beam from the OPO. If these have parallel polarizations, the SFG stage will be type 1 phase matched, and if the polarizations are orthogonal the SFG stage will be type 2 phase matched. Since the beams follow separate paths before being combined in the SFG crystal, the orientation of the polarizations can be chosen by use of a wave plate in one of the beams or by choice of how the pump to the OPO is separated from the rest of the pump (for instance by using a polarizing beam splitter or a partial reflector).

5.1 SFG with 532 nm

The following simulations have been performed with a BBO crystal and assuming d_{22} = 2.6 pm/V and d_{31} = 0.04 pm/V [34, and references therein]. The cutting angles, d_{eff} and walk-off angles for type 1 and 2 PM are summarized in Table 5.1. It should be noted that the effective nonlinearity is smaller for type 2 PM. Therefore, type 2 PM will require a longer BBO crystal than type 1 PM.[7]

PM	θ	φ	d_{eff}	$L\Delta\lambda_1$ (nm·mm)	Walk-off
1	40.5º	30º	1.5	2.8	~ 4.5º (UV)
2	57.1º	0	0.8	2.2	~ 4º (UV+670 nm)

Table 5.1 Parameters for BBO cut for sum-frequency generation of 532 nm and 670 nm to 296 nm [34, and references therein]

In the simulations to optimize the SFG stage, we have used the same pump beam that was used to pump the 532 nm pumped OPO, but scaled the energy (to approximately 80 mJ in most simulations), while the 670 nm output from the OPO simulations has been used as the other input beam. The energy of this beam has been scaled with 0.9 to accommodate for potential loss in optics between the OPO and the SFG stage, leading to about 60 mJ of 670 nm incident on the SFG-crystal. Simulations have been performed both for SLM pump and for MLM pump. In the latter case, a 20 GHz FWHM 532 nm pump has been used for both the OPO and the SFG stage. In all simulations, the peak combined fluence was ~1.6 J/cm^2. In Figure 5.1, the simulated SFG performance is shown as function of BBO length for type 1 PM. We note that a length of 5-6 mm seems optimal for this mode of operation. The reason for the poorer performance at longer crystal lengths is back conversion, which is also evident from the significantly poorer beam quality. Similar results for type 2 PM are shown in Figure 5.2. For this mode of operation, 10-12 mm crystal length seems optimal.

[7] The data in Table 5.1 are calculated from nonlinearities given in Nikogosyan[34]. Another reference indicates that the difference in effective nonlinearity between type 1 and type 2 PM may be significantly larger, ~1.6 pm/V for type 1 PM and ~0.6 pm/V for type 2 PM [23], leading to a larger difference in the optimal BBO crystal length

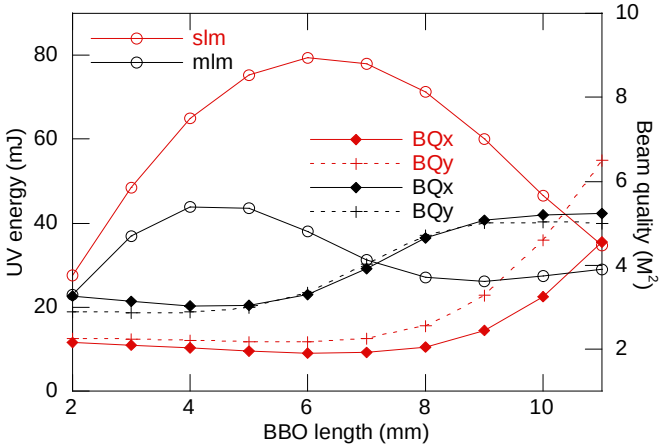

Figure 5.1 SFG performance as function of BBO crystal length for type 1 PM for 80 mJ 532 nm pump and ~60 mJ at 670 nm

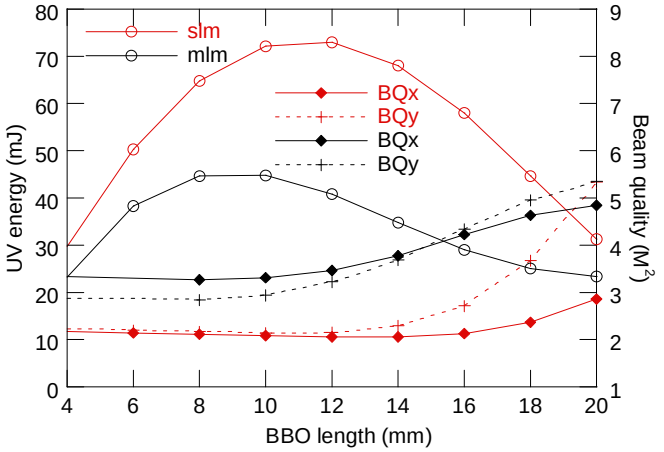

Figure 5.2 SFG performance as function of BBO crystal length for type 2 PM for 80 mJ 532 nm pump and ~60 mJ at 670 nm

The pulse from the OPO is slightly 'delayed' compared to the pump pulse. This stems from the build-up time of the OPO. In a real system this may have to be compensated by adding a delay line for the 532 nm pump. In Figure 5.3, the SFG performance for type 1 PM and a 6 mm long BBO crystal is shown as function of delay of the 670 nm pulse with respect to the 532 nm pulse (negative number means that the 532 nm pulse is delayed). A delay of ~1.5 ns (~50 cm path length) seems to be optimal in this case.

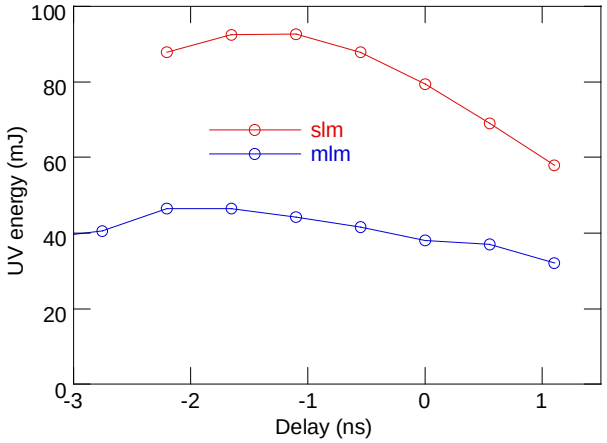

Figure 5.3 SFG performance as function of 670 nm pulse delay relative to the 532 nm pump pulse

Finally, the estimates for the optimal distribution of 532 nm pump energy given in Chapter 4 are tested. The OPO performance was simulated by changing the pump energy of the OPO while keeping the rest of the parameters constant, as is shown in the left graph in Figure 5.4. The simulations of the SFG stage in the right hand graph of Figure 5.4 have been performed while scaling the pump and 670 nm energies according to the results in the left graph. We notice that the estimated distribution of 120 mJ to the OPO and 80 mJ to the SFG stage (assuming 200 mJ total 532 nm pump energy) is a good estimate for both SLM and MLM mode of operation, but it is also clear that the total efficiency of the MLM system only depends weakly on the exact distribution of the pump energy.

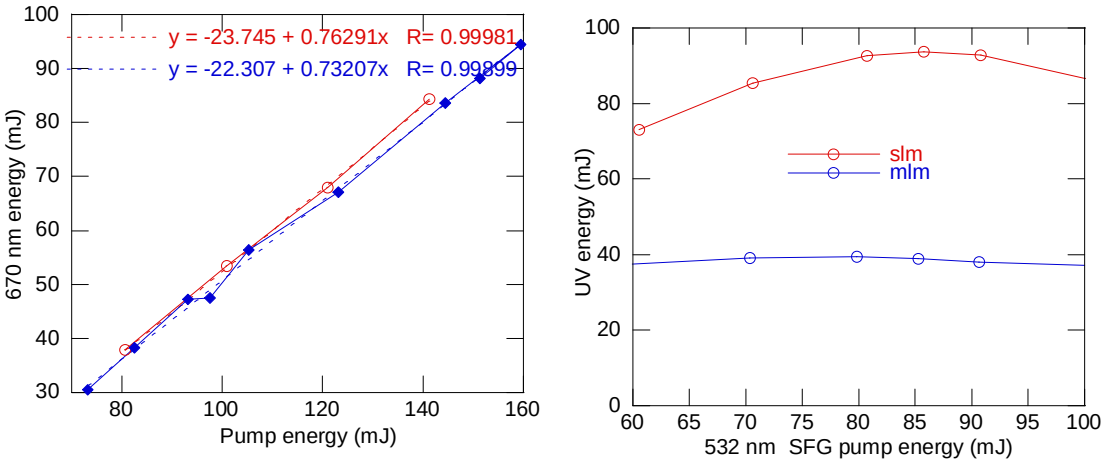

Figure 5.4 Left: OPO performance with SLM (red) or MLM (blue) pumping. Right: SFG performance as function of distribution of pump energy between OPO and SFG stage. 200 mJ total energy assumed in simulations, 670 nm input energy reduced according to left graph when 532 nm energy increases

A final, but important point is that even though the performance of the OPO stage does not depend strongly on the bandwidth of the pump beam, the SFG stage does, and the output UV energy is more than doubled if the OPO-SFG system is pumped with an SLM beam rather than a 20 GHz FWHM bandwidth MLM beam. If possible, SLM operation of the pump laser should therefore be chosen in an experimental setup. The higher sensitivity to pump beam bandwidth in the SFG compared to the OPO, can be explained by the fact that there are two incident beams in the SFG, while the OPO only has one incident beam. If the beams are amplitude modulated, the random spiky temporal nature of the beams will give efficient conversion only at the time when the intensity of both beams are above a certain value, while for an OPO this restriction applies only to one beam. For an SLM-pumped SFG, only one beam is modulated (the beam from the OPO), hence the higher conversion efficiency.

It is worth noting that this analysis is based on the output energies available from the intended pump laser. The harmonic conversion stages of this laser were optimized for high energy at 355 nm. If instead the second-harmonic stage was optimized for 532 nm generation, more than 300 mJ would be available at this wavelength, and considerably more UV energy could be produced. This would, however, also require larger beams, and the beam quality would likely be somewhat poorer.

5.2 SFG with 355 nm

For the SFG stage pumped with 355 nm, the difference between type 1 and type 2 PM in BBO is less, as is shown in Table 5.2.

PM	θ	φ	d_{eff}	$L\Delta\lambda_1$ (nm·mm)	Walk-off
1	30º	30º	1.8	14	~ 3º (UV)
2	32º	0	1.3	12	~ 2.5º (UV+1700 nm)

Table 5.2 Parameters for BBO cut for sum-frequency generation of 355 nm and 1700 nm to 296 nm

In the simulations to optimise the SFG stage, we have assumed that the energy of the 355 nm beam is given by

$$E_{355} = \eta_{355} E_{1064} = \eta_{355} \left(E_L - E_P \right), \qquad (5.1)$$

where η_{355} is the slope efficiency of the 355 nm generation and E_{1064} is the energy at 1064 nm that is not used to pump the OPO, and $E_{1064} = E_L - E_P$, according to (4.2). With the available pump laser, E_L = 600 mJ and η_{355} = 0.33, this leads to E_{355} = 160 mJ since E_P = 120 mJ have been used in most of the simulations. In all simulations, the 1700 nm output from OPO simulations was used as the other beam, with the power scaled to 90% to accommodate for potential loss in coupling optics. As the OPO pulse is significantly shorter than the 355 nm pump pulse (3 ns vs. 5 ns), the pump pulse was delayed 2 ns with respect to the 1700 nm pulse to have the pulses peak at the same time in the BBO crystal. The sensitivity to this delay is shown in Figure 5.7. The 1700 nm energy incident on the BBO crystal was ~30 mJ. In simulations with MLM beams, a

beam with the same modulation pattern that pumped the OPO has been used for the 355 nm beam. Both beams were focused to ~90% diameter to give 1.6 J/cm^2 total peak fluence in the BBO crystal.

In Figure 5.5, the SFG performance is shown as function of BBO length for type 1 PM. We note that a length of 4-5 mm seems optimal for this mode of operation, and that back conversion seems to become important for lengths above 6 mm. Similar results for type 2 PM are shown in Figure 5.6. Even for this mode of operation, ~5 mm crystal length seems optimal.

It is worth noting that the 20 GHz pump bandwidth reduces the output from the SFG stage less with 355 nm pumping than with 532 nm pumping. This is also reflected in the acceptance interval which is significantly larger for the 355 nm pumped SFG, see Tables 5.1-2.

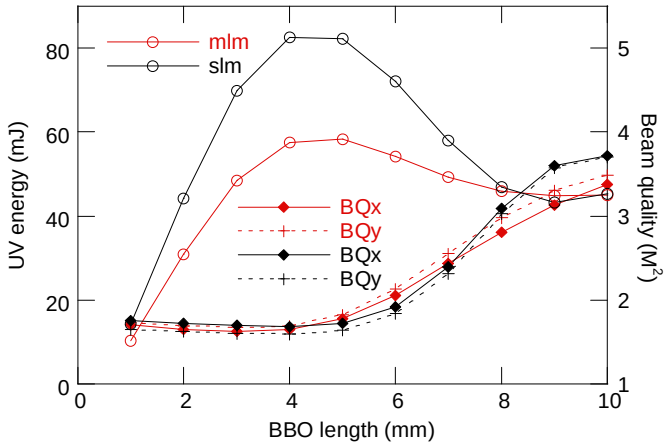

Figure 5.5 Simulated SFG performance as function of BBO length for type 1 PM with 2 ns pump delay with respect to the 1700 nm pulse

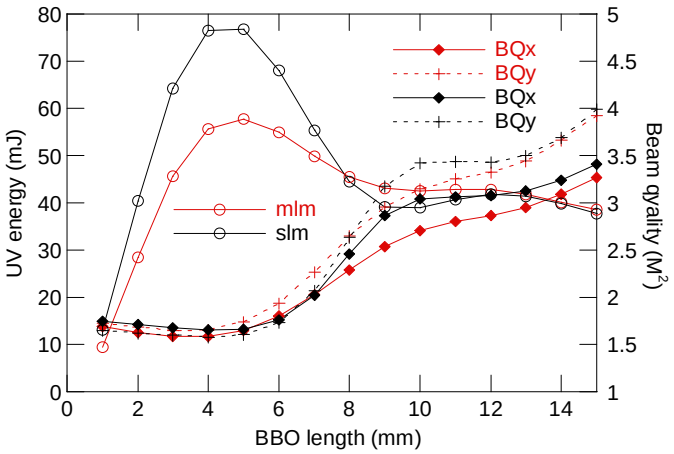

Figure 5.6 Simulated SFG performance as function of BBO length for type 2 PM with 2 ns pump delay with respect to the 1700 nm pulse

The optimal delay between the pump pulse and the pulse from the OPO is even larger that for the 532 nm pumped SFG, and appears to be close to 2.5 ns (or 75 cm) as is shown in Figure 5.7. This is because the pulse from the OPO is significantly shorter than the pump pulse owing to a long build-up time.

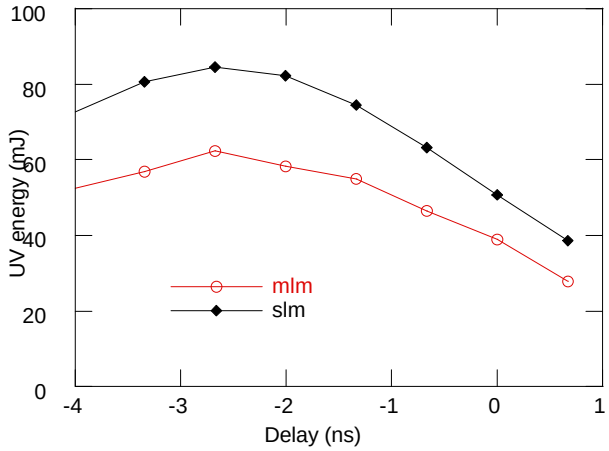

Figure 5.7 Simulated SFG performance as function of 1700 nm pulse delay relative to the pump pulse for type 1 PM with 5 mm BBO crystal length (negative number means that the pump pulse is delayed, positive number means 1700 nm pulse delay)

Finally, we have also studied the optimal distribution of 1064 nm energy, as was also estimated in Chapter 4.1. This was done by varying the pump power used to pump the OPO, and scale the energies in the input beams to the SFG stage accordingly. The energy of the 1700 nm beam was scaled using simulations of the OPO as shown in the left graph in Figure 5.8, while the 355 nm pump energy was scaled according to (5.1). It appears from these simulations that the estimated optimal OPO pump energy of 120 mJ is a good choice.

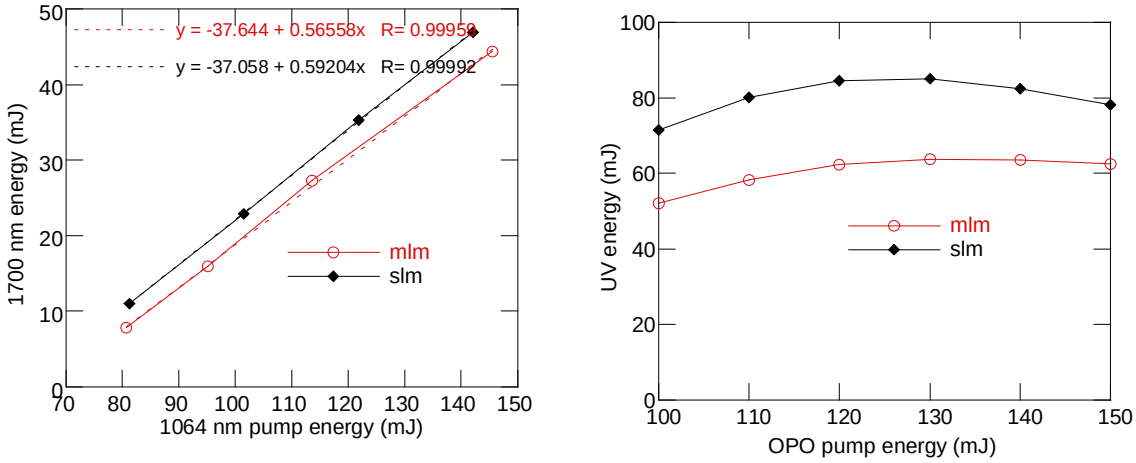

Figure 5.8 Left: OPO performance with SLM (black) or MLM (red) pumping. Right: SFG performance as function of distribution of pump energy between OPO and SFG stage. 200 mJ total energy assumed in simulations, 670 nm input energy reduced according to left graph when 532 nm energy increases

5.3 Alternative materials

BBO seems to be a good choice of material for the SFG stage, based on availability, damage threshold, absorption losses and nonlinearity. The walk-off angle is rather large, but this is not important for the beam sizes and crystals lengths used here. If MLM operation of the pump laser is necessary, a material with higher acceptance bandwidth may be preferred. However, as was seen in [1], the most important materials with higher acceptance bandwidths, LBO and KDP, both have significantly smaller effective nonlinearity (in the range 0.3-0.7 pm/V). A SFG stage with one of these materials would then require a significantly longer crystal which would reduce the actual acceptance bandwidth (inverse proportional with crystal length). Therefore, we consider BBO to be the best choice for the SFG stage.

6 Conclusions

In conclusion, the simulations in this report predict that about 80 mJ of 290-300 nm energy can be generated when starting with 600 mJ at 1064 nm from a single-frequency pump laser. The expected beam quality is in the range $M^2 \sim 2 – 4$. If the pump laser has a 20 GHz bandwidth, the ultraviolet pulse energy is reduced to about 50 mJ. Of the two studied conversion pathways which were described in a previous FFI-Rapport [1], the pathway that includes sum frequency generation of 355 nm and 1700 nm seems to give a slightly better beam quality, while the output energies are about the same. The pathway that includes sum frequency generation of 532 nm and 650 nm, on the other hand, has potential for higher output energy if the commercial harmonic conversion stages were optimized for 532 nm generation.

The beam quality from the high energy optical parametric oscillators (OPOs) were considerably improved by a novel technique that includes the use of two different nonlinear crystals in the

same resonator to narrow down the far field of the signal beam in both transversal directions. Using the nonlinear materials BBO and KTA, a symmetrical beam with 30 mJ pulse energy and $M^2 \sim 2$ at 1700 nm and with ~60 mJ pulse energy and $M^2 < 3$ at 650 nm was obtained in very simple linear resonators. It was also found that for maximum generated energy in the ultraviolet, 120 mJ of either the 600 mJ available at 1064 nm or the 200 mJ available at 532 nm should be used to pump the OPO, while the rest of the pump energy should be used for the other beam in the sum frequency generation stage.

Simulations of Master Osillator – Power Amplifier alternatives to the high energy OPOs resulted in slightly better performance in terms of energy for the 1700 nm beam and beam quality for the 650 nm beam. However, the added complexity of the experimental setup of these architectures still makes the high energy OPOs the recommended choice for the application studied in this report.

References

[1] G Rustad and Ø Farsund (2008). *Evaluation of methods and materials for optical generation of high pulse energies at 290 nm*. FFI-rapport 2008/02107, FFI, Kjeller. www.ffi.no

[2] G Arisholm. General numerical methods for simulating second-order nonlinear interactions in birefringent media. *J. Opt. Soc. Am. B*, 14: 2543-2549, 1997. DOI: 10.1364/JOSAB.14.002543

[3] G Arisholm. Advanced numerical simulation models for second-order nonlinear interactions. *Proc. SPIE*, 3685: 86-97, 1999. DOI: 10.1117/12.335826

[4] G Arisholm. Quantum noise initiation and macroscopic fluctuations in optical parametric oscillators. *J. Opt. Soc. Am. B*, 16: 117-127, 1999. DOI: 10.1364/JOSAB.16.000117

[5] H Kouta. Wavelength dependence of repetitive-pulse laser-induced damage threshold in β-BaB_2O_4. *Appl. Opt.*, 38: 545-547, 1999. DOI: 10.1364/ao.38.000545

[6] G Rustad, G Arisholm, and Ø Farsund. Effect of idler absorption in pulsed optical parametric oscillators. *Opt. Express*, 19: 2815-2830, 2011. DOI: 10.1364/OE.19.002815

[7] Y R Shen. *The principles of nonlinear optics*. Wiley, New York, 1984. ISBN: 0-471-88998-9.

[8] G Arisholm, E Lippert, G Rustad, and K Stenersen. Efficient conversion from 1 to 2 µm by a KTP-based ring optical parametric oscillator. *Opt. Lett.*, 27: 1336-1338, 2002. DOI: 10.1364/ol.27.001336

[9] S Chandra, T H Allik, and J A Hutchinson. Nonfocal unstable resonator for solid-state dye-lasers based on a gradient-reflectivity mirror. *Opt. Lett.*, 20: 2387-2389, 1995. DOI: 10.1364/OL.20.002387

[10] B C Johnson, V J Newell, J B Clark, and E S McPhee. Narrow-bandwidth low-divergence optical parametric oscillator for nonlinear frequency-conversion applications. *J. Opt. Soc. Am. B*, 12: 2122-2127, 1995. DOI: 10.1364/JOSAB.12.002122

[11] S Pearl, Y Ehrlich, S Fastig, and S Rosenwaks. Nearly Diffraction-Limited Signal Generated by a Lower Beam-Quality Pump in an Optical Parametric Oscillator. *Appl. Opt.*, 42: 1048-1051, 2003. DOI: 10.1364/AO.42.001048

[12] G Arisholm, O Nordseth, and G Rustad. Optical parametric master oscillator and power amplifier for efficient conversion of high-energy pulses with high beam quality. *Opt. Express*, 12: 4189-4197, 2004. DOI: 10.1364/opex.12.004189

[13] D J Armstrong and A V Smith. 150-mJ 1550-nm KTA OPO with good beam quality and high efficiency. *Proc. SPIE*, 5337: 71-80, 2004. DOI: 10.1117/12.528436

[14] G Rustad and Ø Farsund (2008). *Standoff detection of biological aerosols by UV-laser induced fluorescence*. FFI-Rapport 2008/02025, FFI, Kjeller. www.ffi.no

[15] A V Smith and M S Bowers. Image-rotating cavity designs for improved beam quality in nanosecond optical parametric oscillators. *J. Opt. Soc. Am. B*, 18: 706-713, 2001. DOI: 10.1364/JOSAB.18.000706

[16] D J Armstrong and A V Smith. All solid-state high-efficiency tunable UV source for airborne or satellite-based ozone DIAL systems. *IEEE J. Sel. Top. Quantum Electron.*, 13: 721-731, 2007. DOI: 10.1109/JSTQE.2007.896600

[17] G Arisholm, E Lippert, G Rustad, and K Stenersen. Effect of resonator length on a doubly resonant optical parametric oscillator pumped by a multilongitudinal-mode beam. *Opt. Lett.*, 25: 1654-1656, 2000. DOI: 10.1364/OL.25.001654

[18] G Rustad, E Lippert, K Stenersen, and G Arisholm. Enhanced power from a doubly resonant optical parametric oscillator by choice of resonator length. In: *Advanced Solid-State Lasers*, Trends in Optics and Photonics Series vol 50, C Marshall, ed (Optical Soc America, 2001), pp 660-665.

[19] A V Smith, D J Armstrong, and W J Alford. Increased acceptance bandwidths in optical frequency conversion by use of multiple walk-off-compensating nonlinear crystals. *J. Opt. Soc. Am. B*, 15: 122-141, 1998. DOI: 10.1364/JOSAB.15.000122

[20] C D Nabors and G Frangineas. Optical parametric oscillator with bi-noncolinear, porro prism cavity. In: *Advanced Solid State Lasers*, Trends in Optics and Photonics vol 10, C R Pollock and W R Bosenberg, eds (Optical Society of America, 1997), pp 90-93.

[21] G Anstett, G Goritz, D Kabs, R Urschel, R Wallenstein, and A Borsutzky. Reduction of the spectral width and beam divergence of a BBO-OPO by using collinear type-II phase matching and back reflection of the pump beam. *Appl. Phys. B*, 72: 583-589, 2001. DOI: 10.1007/s003400100533

[22] V Pasiskevicius, H Karlsson, F Laurell, R Butkus, V Smilgevicius, and A Piskarskas. High-efficiency parametric oscillation and spectral control in the red spectral region with periodically poled $KTiOPO_4$. *Opt. Lett.*, 26: 710-712, 2001. DOI: 10.1364/OL.26.000710

[23] W J Alford and A V Smith. Wavelength variation of the second-order nonlinear coefficients of $KNbO_3$, $KTiOPO_4$, $KTiOAsO_4$, $LiNbO_3$, $LiIO_3$, β-BaB_2O_4, KH_2PO_4, and LiB_3O_5 crystals: a test of Miller wavelength scaling. *J. Opt. Soc. Am. B*, 18: 524-533, 2001. DOI: 10.1364/JOSAB.18.000524

[24] K Kato and E Takaoka. Sellmeier and thermo-optic dispersion formulas for KTP. *Appl. Opt.*, 41: 5040-5044, 2002. DOI: 10.1364/AO.41.005040

[25] D L Fenimore, K L Schepler, U B Ramabadran, and S R McPherson. Infrared Corrected Sellmeier Coefficients for Potassium Titanyl Arsenate. *J. Opt. Soc. Am. B*, 12: 794-796, 1995. DOI: 10.1364/JOSAB.12.000794

[26] D Eimerl, L Davis, S Velsko, E K Graham, and A Zalkin. Optical, Mechanical, and Thermal-Properties of Barium Borate. *J. Appl. Phys.*, 62: 1968-1983, 1987. DOI: 10.1063/1.339536

[27] M Ghotbi and M Ebrahim-Zadeh. Optical second harmonic generation properties of BiB_3O_6. *Opt. Express*, 12: 6002-6019, 2004. DOI: 10.1364/OPEX.12.006002

[28] N Umemura, K Miyata, and K Kato. New data on the optical properties of BiB_3O_6. *Opt. Mat.*, 30: 532-534, 2007. DOI: 10.1016/j.optmat.2006.12.014

[29] M V Pack, D J Armstrong, A V Smith, G Aka, B Ferrand, and D Pelenc. Measurement of the χ^2 tensor of $GdCa_4O(BO_3)_3$ and $YCa_4O(BO_3)_3$ crystals. *J. Opt. Soc. Am. B*, 22: 417-425, 2005. DOI: 10.1364/JOSAB.22.000417

[30] N Umemura, H Nakao, H Furuya, M Yoshimura, Y Mori, T Sasaki, K Yoshida, and K Kato. 90 degrees phase-matching properties of $YCa_4O(BO_3)_3$ and $Gd_xY_{1-x}Ca_4O(BO_3)_3$. *Jpn. J Appl. Phys. Part 1*, 40: 596-600, 2001. DOI: 10.1143/JJAP.40.596

[31] D H Jundt, M M Fejer, and R L Byer. Optical-Properties of Lithium-Rich Lithium-Niobate Fabricated by Vapor Transport Equilibration. *IEEE J. Quantum Electron.*, 26: 135-138, 1990. DOI: 10.1109/3.44926

[32] D A Roberts. Simplified Characterization of Uniaxial and Biaxial Nonlinear Optical-Crystals - a Plea for Standardization of Nomenclature and Conventions. *IEEE J. Quantum Electron.*, 28: 2057-2074, 1992. DOI: 10.1109/3.159516

[33] K Kato. Temperature-tuned 90º phase matching properties of LiB_3O_5. *IEEE J. Quantum Electron.*, 30: 2950-2952, 1994. DOI: 10.1109/3.362711

[34] D N Nikogosyan. *Nonlinear optical crystals: a complete survey*. Springer, New York, 2005. ISBN: 0387220224.

[35] F Zernike, Jr. Refractive indices of ammonium dihydrogen phosphate and potassium dihydrogen phosphate between 2000Å and 1.5 μm. *J. Opt. Soc. Am.*, 54: 1215-1220, 1964. DOI: 10.1364/JOSA.54.001215

[36] E C Cheung, K Koch, G T Moore, and J M Liu. Measurements of second-order nonlinear optical coefficient from the spectral brightness of parametric fluorescence. *Opt. Lett.*, 19: 168-170, 1994. DOI: 10.1364/OL.19.000168

[37] E Takaoka and K Kato. Thermo-optic dispersion formula for $AgGaS_2$. *Appl. Opt.*, 38: 4577-4580, 1999. DOI: 10.1364/AO.38.004577

[38] W Koechner. *Solid-state laser engineering*. Springer, New York, 2006. ISBN: 978-0-387-29094-2.

[39] J P Feve, B Boulanger, O Pacaud, I Rousseau, B Menaert, G Marnier, P Villeval, C Bonnin, G M Loiacono, and D N Loiacono. Phase-matching measurements and Sellmeier equations over the complete transparency range of $KTiOAsO_4$, $RbTiOAsO_4$, and $CsTiOAsO_4$. *J. Opt. Soc. Am. B*, 17: 775-780, 2000. DOI: 10.1364/josab.17.000775

[40] D X Zhang, Y F Kong, and J Y Zhang. Optical parametric properties of 532-nm-pumped beta-barium-borate near the infrared absorption edge. *Opt. Commun.*, 184: 485-491, 2000. DOI: 10.1016/s0030-4018(00)00968-8

Appendix A List of Abbreviations

Acronym	Explanation
BBO	β-BaB_2O_4 – Beta-Barium Borate
BQ	Beam quality
BQx/BQy	Beam quality in the x/y direction
DRO	Doubly resonant oscillator
e-pol	Extraordinary polarization
FOV	Field of view
FWHM	Full width at half maximum
IR	(here) Idler removal
KDP	KH_2PO_4 - Potassium Dihydrogen Phosphate
KTA	$KTiOAsO_4$ - Potassium Titanyl Arsenate
KTP	$KTiOPO_4$Potassium Titanyl Phosphate
LBO	LiB_3O_5 - Lithium Triborate
mJ	Millijoule, 10^{-3} J
MLM	Multi longitudinal mode
MOPA	Master oscillator power amplifier
mrad	Milliradian, 0.001 rad (≈ 0.057º)
ng (or n_g)	Group index
ns	Nanosecond, 10^{-9} s
OPA	Optical parametric amplifier
OPO	Optical parametric oscillator
o-pol	Ordinary polarization
pm	Picometer, 10^{-12} m
PM	Phase matching
SFG	Sum frequency generation
SLM	Single longitudinal mode
SRO	Singly resonant oscillator
UV	Ultraviolet

Appendix B Acceptance intervals

In nonlinear optics, the acceptance interval for a parameter expresses how sensitive PM and nonlinear gain are to a change in the particular parameter, and is usually defined as

$$L\Delta\xi = \frac{5.56}{\left| d\Delta\vec{k}/d\xi \right|}, \tag{B.1}$$

where ξ is the parameter to be varied, Δk is the phase mismatch and L is the crystal length. The factor of 5.56 is the distance between the first order zero points for the sinc^2-function.

In Table 3.1-2, the acceptance interval for the signal angle was calculated to indicate how narrow the angular spectrum of the signal beam may be expected to be for various nonlinear materials. In the calculations, we have assumed the signal and idler wavelengths to be fixed, and that the idler angle adapts to minimize the phase mismatch when the signal angle varies. We have also taken into account that the signal and idler refractive indexes vary with angle. This is solved numerically, and the derivative at zero angle is found. In Figure B.1, the calculated phase mismatch is shown for type 1 and type 2 PM in BBO for the interaction 532 nm → 650 nm + 2930 nm. As expected, the OPO is far less sensitive for signal angle under type 1 PM than for type 2 PM, resulting in a much larger (in this case a singularity) acceptance bandwidth for the signal angle.

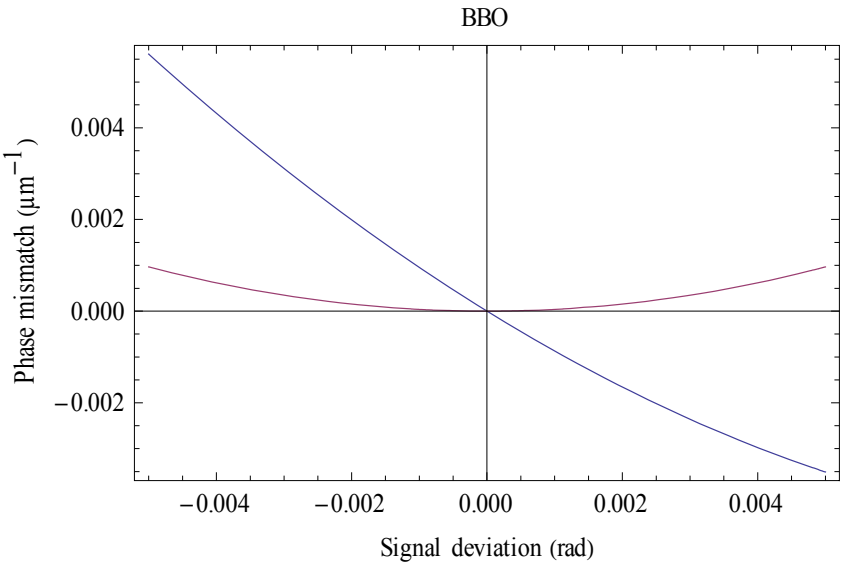

Figure B.1 Calculated phase mismatch (Δk) as function of angle between signal and pump for type 1 (red curve) and type 2 (blue curve) PM in BBO for the process 532 nm -> 650 nm + 2930 nm